Science of the Total Environment 801 (2021) 149712

Contents lists available at ScienceDirect

Science of the Total Environment

journal homepage: www.elsevier.com/locate/scitotenv

Offshore benthic habitat mapping based on object-based image analysis and geomorphometric approach. A case study from the Slupsk Bank, Southern Baltic Sea

Lukasz Janowski [a,*], Radoslaw Wroblewski [b,c], Janusz Dworniczak [c], Mateusz Kolakowski [c], Karolina Rogowska [c], Michal Wojcik [d], Juliusz Gajewski [a]

[a] Maritime Institute, Gdynia Maritime University, Dlugi Targ 41/42, 80-830 Gdansk, Poland
[b] Institute of Geography, University of Gdansk, Bazynskiego 4, 80-309 Gdansk, Poland
[c] MEWO S.A, Starogardzka 16, 83-010 Straszyn, Poland
[d] Department of Computer Architecture, Faculty of Electronics, Telecommunications and Informatics, Gdansk University of Technology, Gabriela Narutowicza 11/12, 80-233 Gdansk, Poland

HIGHLIGHTS

- Automatic classifications are essential for benthic habitat mapping of vast areas.
- Hydroacoustics allowed combining data from hydrosphere, lithosphere and biosphere.
- The workflow, including object-oriented and geomorphometric approach, was developed.
- The first acoustic datasets of the Slupsk Bank allowed assessment of the model.
- There is a need to develop novel predictor variables for benthic habitat mapping.

GRAPHICAL ABSTRACT

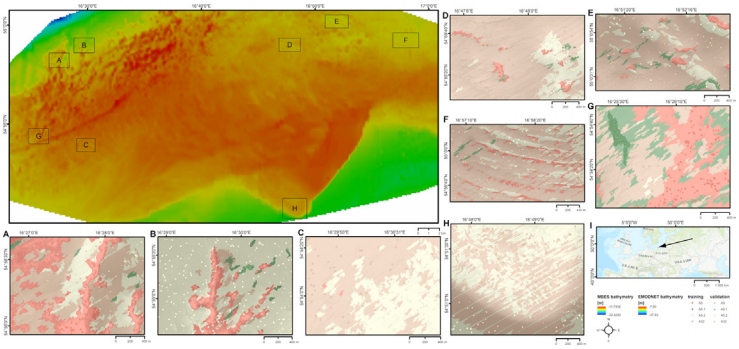

ARTICLE INFO

Article history:
Received 14 June 2021
Received in revised form 28 July 2021
Accepted 12 August 2021
Available online 18 August 2021

Editor: Martin Drews

Keywords:
Benthic habitat mapping
Multibeam echosounder
Side-scan sonar
Object-based image analysis
Feature selection
Geomorphometry

ABSTRACT

Benthic habitat mapping is a rapidly growing field of underwater remote sensing studies. This study provides the first insight for high-resolution hydroacoustic surveys in the Slupsk Bank Natura 2000 site, one of the most valuable sites in the Polish Exclusive Zone of the Southern Baltic. This study developed a quick and transparent, automatic classification workflow based on multibeam echosounder and side-scan sonar surveys to classify benthic habitats in eight study sites within the Slupsk Bank. Different predictor variables, four supervised classifiers, and the generalisation approach, improving the accuracy of the developed model were evaluated. The results suggested a very high significance for the classification performance of specific geomorphometric features that were not used in benthic habitat mapping before. These include, e.g., Fuzzy Landform Element Classification, Multiresolution Index of the Valley Bottom Flatness, and Multiresolution Index of the Ridge Top Flatness. Comparison of classification results with manual maps demonstrated that Random Forest had the highest performance of four tested supervised classifiers. Because the current needs include benthic habitat mapping for the whole area of the Polish Exclusive Economic Zone, the key findings of this study may be further applied to extensive areas in the Polish waters and other vast areas worldwide.

* Corresponding author.
E-mail addresses: ljanowski@im.umg.edu.pl (L. Janowski), radoslaw.wroblewski@ug.edu.pl, rwroblewski@mewo.eu (R. Wroblewski), jdworniczak@mewo.eu (J. Dworniczak), mkolakowski@mewo.eu (M. Kolakowski), krogowska@mewo.eu (K. Rogowska), michal.wojcik@eti.pg.edu.pl (M. Wojcik), juliusz.gajewski@im.umg.edu.pl (J. Gajewski).

https://doi.org/10.1016/j.scitotenv.2021.149712

1. Introduction

Because most of the ocean floor is still not explored (Wölfl et al., 2019), mapping the seabed is currently an essential task to ensure continuity of high-resolution maps for the entire planet. The extensive international programs aim to change this state of knowledge. Examples include recently launched activities, such as GEBCO Seabed 2030 (Mayer et al., 2018), Shell Ocean Discovery XPRIZE (Zwolak et al., 2020), as well as national programs operating for many years, like MAREANO (Bøe et al., 2020), MAREMAP (Howe et al., 2015), and INFOMAR (Guinan et al., 2021). Detailed maps of the seabed are critical for multiple tasks, like sustainable development, underwater archaeology (Pydyn et al., 2021), and environmental protection (Harris and Baker, 2012). Whereas 'Healthy Oceans' is one of five key challenges facing the EU included in the Horizon Europe Programme, the current period was named by United Nations as the Decade of Ocean Science for Sustainable Development (Ryabinin et al., 2019). All the initiatives mentioned above demonstrate the extreme importance of mapping the ocean to preserve its resources for future generations.

Natura 2000 Special Protection Areas include European territories of the most special ecological interest. One of the most valuable offshore ecological Natura 2000 areas in the Polish Exclusive Zone of the Southern Baltic is the Slupsk Bank. Covering 800 km^2, the area was inscribed under the PLC 990001 number forming a unique area of birds and habitats protection. Slupsk Bank is known for its numerous boulder deposits, ideal for the development of benthic habitats (Andrulewicz et al., 2004). Whereas the area has essential ecological quality, until now, its bathymetry was still unpublished. This research paper presents the first results of benthic habitat mapping of the Slupsk Bank based on high-resolution hydroacoustic surveys. Because the current needs of the Polish Chief Inspectorate of Environmental Protection include benthic habitat mapping for the whole area (25,000 km^2) of the Polish waters, the methods proposed in this study can be further applied to potentially much larger areas in the Polish Exclusive Economic Zone.

Recent advances in the development of hydroacoustics and big data processing methods have enabled the rapid growth of benthic habitat mapping and exploration of the seabed. Multibeam echosounders (MBES), as well as side-scan sonars (SSS), allow measuring bathymetry and seabed characteristics in a high-resolution and relatively short time. Machine learning algorithms enable the seabed classification based on full coverage hydroacoustic surveys and additional ground-truth datasets (Brown et al., 2011). More recently, the spatial determination of benthic habitats has been facilitated by Object-Based Image Analysis (OBIA), widely known in terrestrial remote sensing studies (Diesing et al., 2016). Furthermore, the recent advances of benthic habitat mapping include improvement of classification models by implementing oceanographic variables (Pearman et al., 2020), integrating geomorphometric features of the seafloor (Lecours et al., 2016), determining new predictor variables (Trzcinska et al., 2020), a multi-scale approach (Misiuk et al., 2021), and ensemble modeling (Georgian et al., 2019). In this work, we developed the automatic classification models for the Slupsk Bank based on the OBIA approach. We evaluated the suitability of multiple morphometric predictor variables from terrestrial remote sensing for benthic habitat mapping. Additionally, we tested the performance of four supervised classification models as well as the impact of map generalisation on classification accuracy. Geomorphologic characteristics of the seafloor relief with its cartographic representation are a basic set of indicators of environmental conditions and their changes. These data are essential for all purposes of exploration and definition of the nature of the bottom for research and application, including benthic habitat assessment, natural resource exploration and exploitation, suitability for technical infrastructure assessment, and other specialised purposes (Rudowski et al., 2019).

This research aims to answer the following research questions: (a) How object-based image analysis can support the automatic classification of benthic habitats based on underwear acoustic measurements? (b) How can different predictor variables and various classifiers improve the accuracy of automated classification of benthic habitats? (c) Can a single classification model be successfully applied to a few geomorphologically different areas of shallow bathymetry? (d) Does the generalisation of classification results affect the accuracy of benthic habitat maps? The structure of this paper has been organised as follows. The next section describes the study area, procedures of hydroacoustic data acquisition and processing, and details of manual and automatic determination of benthic habitats. The Results section includes outcomes of feature selection, evaluation of classification models in the eight study sites, and estimations of accuracy. The discussion was separated for the in-depth quantitative and qualitative interpretation of results, implications of the results, study limitations, and future perspectives.

2. Materials and methods

2.1. Study site

The Slupsk Bank is a shallow area of the Southern Baltic Sea, located at a distance of approximately 20–25 km north of the Polish coast, in the vicinity of the Ustka town. The seafloor relief of the Slupsk Bank is an effect of geomorphological processes of glacial origin in Pleistocene as well as terrestrial and marine origin in Holocene. Relatively recently, approximately 7000 years ago, a significant area of the Slupsk Bank still emerged above sea level. After the Littorina transgression, the area was submerged underwater. The unique character of the Slupsk Bank distinguishes the area from other regions of the southern Baltic Sea.

The analysed area of the seabed varies in depth from approximately 8.0 to approximately 38.0 m. The shallowest parts of the bottom include the northern and northwestern parts of the area (minimum depth of about 8.0 m b.s.l.) and parts of the sandy bottom of the central part of the area (minimum depth of about 12.0 m b.s.l.). The bottom surface decreases in all directions around the indicated shallowest parts of the study area. The deepest parts of the bottom (up to approximately 38 m b.s.l.) are located in the southeastern part of the area.

The northwestern part of the Slupsk Bank seafloor has prominent glacial relief, with depths ranging from about 8.0 m to more than 30 m b.s.l., with the most diverse relief. The depth of the bottom in this part increases towards the north. Tills form the seafloor surface with a sandy and stony cover with numerous boulders. The bottom relief is dominated by a series of till ridges with a stony cover. The ridge axes generally run in SW–NE direction, forming mainly De Geer moraines (Blake, 2000; Kotilainen et al., 2012; Todd, 2016) and numerous till outcrops in the form of long ridges. These formations reach heights of up to 7–8 m above the surface.

The north-eastern part of the Slupsk Bank is an area with depth from about 15.0 to about 27.0 m b.s.l., with distinct glacial relief and sequences of low, isolated rises. These are mainly hummocky moraine rises and till outcrops. The height of the hills is up to 3–4 m above the surrounding seabed. In the eastern part, there is a field with a series of low De Geer moraine forms (Blake, 2000; Kotilainen et al., 2012; Todd, 2016).

The central and southern part of the Slupsk Bank is an area of extensive sandy areas, covering the bottom with depths ranging from approximately 15.0 to 38.0 m b.s.l. Within this area, a distinct slope separates the shallower parts of the sandy bottom with depths of about 13.0–20.0 m b.s.l. from the sandy and sandy-silty bottom of the deepest parts of the southern and southeastern part of the area (Fig. 1). The slope locally reaches 12–13 m with inclination up to 12–13°.

The sedimentary cover of the Slupsk Bank bottom is formed from Pleistocene glacial, fluvioglacial and limnoglacial sediments, as well as Holocene lake and marine sediments with a thin, discontinuous, diverse cover of recent marine sediments.

2.2. Hydroacoustic datasets

Bathymetric surveys with an MBES were conducted by Przemyslaw Zeranski, Agnieszka Zawieja, Adrian Wraclawek, Michal Franczak and

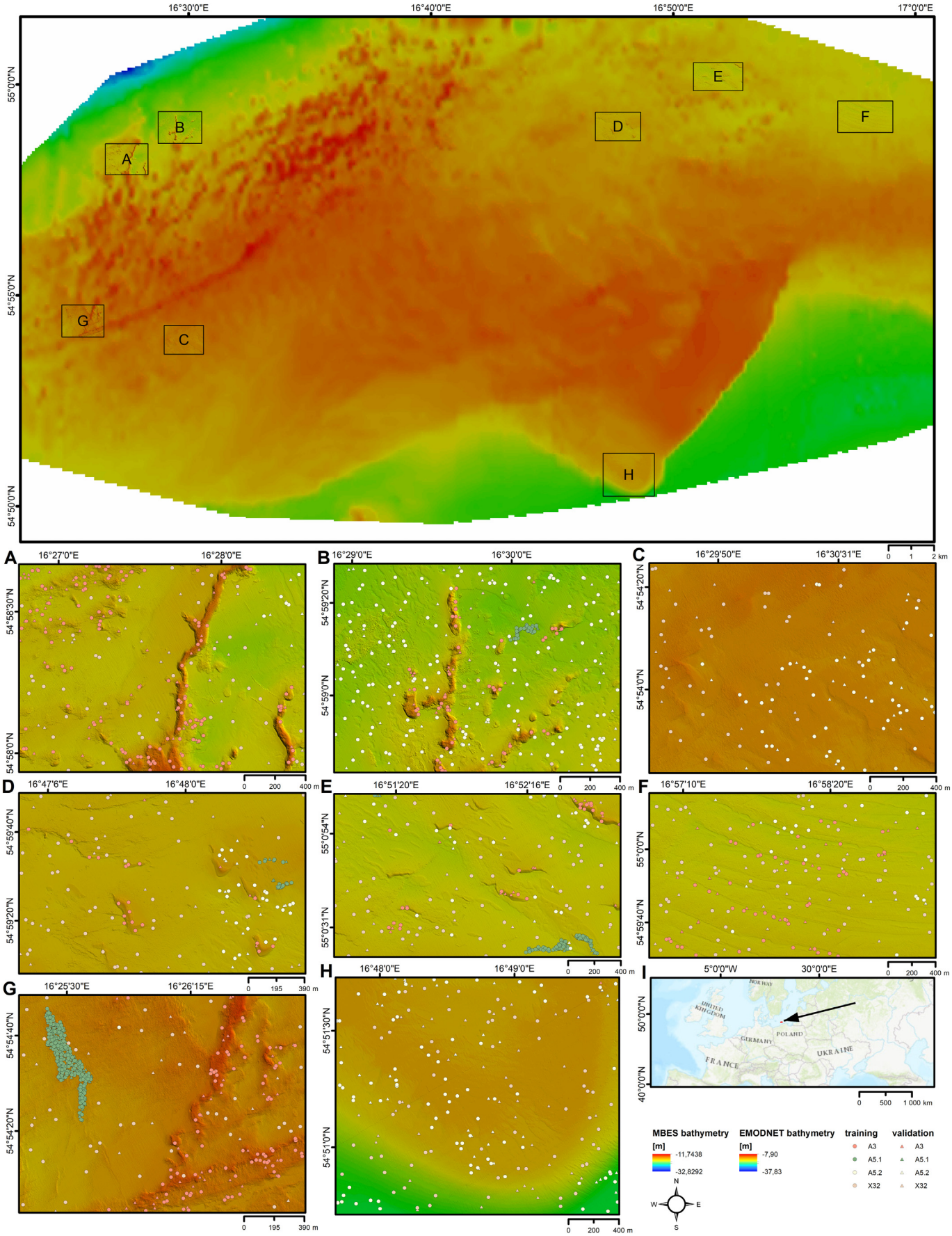

Fig. 1. Location of the study sites (a–h) within the EMODnet bathymetry (EMODnet Bathymetry Consortium, 2020) of Slupsk Bank Natura2000 area (the northern map). (a–h) High-resolution bathymetry maps of eight study sites overlapped with training and validation ground-truth samples; (i) Location of the Slupsk Bank (black arrow) within Europe.

Marta Grabinska in spring 2019 from the R/V MEWO Navigator. Measurements were made at a constant speed of approximately 2 m/s (±10%). They were performed in a way to ensure full bottom coverage. Depending on the depth, the measurement lines were planned every 60 m and 80 m. The primary measurement system was a SeaBat T20-P MBES from Teledyne Reson manufacturer. The applied settings of the MBES were as following: 512 beams; 400 kHz operating frequency; 120° swath coverage; 45 μs pulse length; 50 Hz max ping rate. The Sound Velocity Sensor (SVS), MIDAS CTD Valeport SAIV SD214, was located at the level of the MBES transducer. The HYDRINS from iXBlue (manufactured by 34 rue de la Croix de Fer, CS 70121 Cedex 78105 Saint-Germain en Laye, France) was used for pitch, roll and heading corrections of the vessel. The software used for bathymetric data acquisition was QINSy 8.15 software (manufactured by Quality Positioning Services BV (QPS), Handelsweg 6-2, 3707NH Zeist, Netherlands). The obtained bathymetric data were corrected considering the current sea level (DGPS RTK height measurement) and sound velocity in water. The total error of depth measurements with such a system did not exceed 0.2 m. The data were collected regarding the EGM 2008 ellipsoid, which corresponds to the Kronstadt 86 level.

The bathymetric survey data were processed to remove acoustic noise, validate sea-level changes, and be subject to quality control. The processing of bathymetric data was carried out in two stages. In the first stage, the QINSy 8.15 software was used to perform the analysis and possible correction of data from individual devices. In the second stage, the output data were subjected to further data analysis and cleaning in AutoClean 2.1.0 software (BeamworX B.V., Emmalaan 4, 3581 HR Utrecht, Netherlands). Final cleaned datasets were exported to grid data containing *x*, *y* coordinates and *z* value as a depth with a spatial resolution of 0.5 m. The procedure also included extraction of raw MBES measurements of Bottom Backscatter Strength (BBS) with the same spatial resolution.

The SSS surveys were conducted with the EdgeTech 4200 SSS to provide complete (200%) bottom coverage. The SSS operated at 600 kHz and 900 kHz. The survey lines were planned every 80 m and 60 m allowing covering the SSS swath range of 100 m per channel. The set of side-scan sonar transducers was towed in a way that allowed its good stabilisation in water depth. The sonar position was determined in real-time using the Scout Pro ultra-short baseline (USBL) acoustic positioning system. The survey equipment was calibrated according to the QPS and Autopatch manuals (BeamworX B.V., Emmalaan 4, 3581 HR Utrecht, Netherlands). Digital data from the side-scan sonar were stored in the Coda GeoSurvey sonar data collection and processing system (Coda Octopus Products, Limited, 38 S. Gyle Crescent, South Gyle Business Park, Edinburgh EH12 9EB, United Kingdom). The sonar mosaic was created using Coda GeoSurvey Mosaic software. The sonar mosaics were created by applying filters that sharpened the edges of the forms at the bottom and then smoothing the image. The data were geometrically corrected to remove nadir (the dead zone under the transducer). To achieve uniformity in the sonar image, it was necessary to adjust the strength of the gain of the signal transmitted by the sonar. The resulting SSS images had a spatial resolution of 0.2 m.

2.3. Manual classification of benthic habitats

Manual classification of benthic habitats was performed based on a complete analysis of bathymetric and side-scan sonar data, using available literature and cartographic data, based on extensive knowledge and expert experience. The character of the seabed and the main types of surface sediments were recognized. Based on the interpretation of bathymetric data, a geomorphological sketch was prepared. The sketch contains a set of data on the identified formations, including their genesis. The geomorphological data in combination with sonar data allowed identification of the main groups of sediments building particular forms of the seabed and indication of the range of occurrence of specific types of sediments. On this basis, a surface sediment map was created. The map of surface sediments combined with bathymetric, geomorphological and sonar data were used to create benthic habitat maps. We applied the European Nature Information System (EUNIS) habitat classification scheme, level 3 (Davies et al., 2004). Our benthic habitat maps include the following classes.

A5.1 Sublittoral coarse sediment - coarse sediment in the sublittoral zone. The seabed structure is dominated by gravel, locally thin discontinuous sand covers, isolated pebbles, and single boulders.

A5.2 Sublittoral sand - sands in the sublittoral zone. The surface sediments are mainly fine to medium-grained sand. It forms flat surfaces over most of the bottom surface, with locally occurred ripple marks.

A3 Infralittoral rock and other hard substrata - hard substrate in the infralittoral zone. Clusters of boulders, accumulations of gravel, outcrops of till with erosive pavements on the surface, occasional thin discontinuous sand cover. Most often, this class was observed on the ridges of various types of formations.

X32 Mosaics of mobile and non-mobile substrata in the infralittoral zone. The bottom is often composed of sandy sediments with accumulations of coarser fractions on the surface - gravels, single boulders, and ripple marks. This type of bottom also includes areas with an eroded sandy bottom and exposed substrate rocks of various kinds - from smooth, built from silts and clays, through rough till surfaces to accumulations and patches of gravels with single boulders. A mosaic substrate is varied, composing the other three types of benthic habitats, but occur on small areas of up to several tens of m^2.

The benthic habitat map at a scale of 1:25,000 was developed. Following good practices used for geologic and geomorphologic mapping, analyses of MBES, BBS, and SSS data were conducted on larger scale maps. This work was performed on data at scales of 1:10,000 and larger.

Recognized and interpreted habitats were subjected to verification by performing in situ control observations by a diver or using an ROV system. To obtain the most uniform and consistent benthic habitat map, the classification was performed by a single interpreter. Separations were made during one cycle/interpretation period, which lasted two days. On the first day, interpretation was conducted, and on the second day, the uniformity and consistency of the implemented separations were checked.

2.4. Development of the automatic classification workflow

The automatic workflow developed in this research consisted of several actions that only needed to be done once and other activities that may be performed repeatably to find the best parameters of the model. All calculations were performed on a mobile workstation equipped with AMD Ryzen 7 4800H CPU (2.90–4.2 GHz, 8 cores/16 threads), NVIDIA GeForce RTX 2060 GPU (6GB DDR6), 32GB RAM DDR4 3200 MHz, and M.2 NVMe SSD drive. The details of the workflow were described below.

2.4.1. Generation of random ground-truth points

The manual map of benthic habitats allowed us to generate random ground-truth points in ArcGIS software. For each benthic habitat type, we created 500 points with a minimum allowed distance of 5 m. Additionally, random points of the specified habitat type were generated with a minimum 10 m distance from other habitat types. Considering four classes of habitats, the total number of randomly created points was 2000. The ground-truth dataset was randomly separated with a 70/30 ratio for training and test (validation) subsets using the Subset Features tool in ArcGIS. The exact locations of all points with separation for training and validation subsets are visible in Fig. 1A–H.

2.4.2. Image segmentation

The MBES bathymetry and SSS image (all RGB channels) were used to generate image objects in eCognition 9.0 software (manufactured by Trimble Inc., 935 Stewart Drive Sunnyvale, CA 94085, USA). The algorithm used for the generation of image objects was multiresolution

segmentation. The working principle of the algorithm is an iterative merging of image pixels with similar properties. The similarity is expressed by several parameters, like color/shape and smoothness/compactness, described in detail in Benz et al. (2004). The parameter affecting the size of image objects is scale, which expresses dimensionless value regarding image objects similarity and the image's pixel resolution (Benz et al., 2004). We chose the following from different tested multiresolution segmentation settings: scale 150, shape 0.1, compactness 0.5.

2.4.3. Feature extraction

Independently of ground-truth points generation, we extracted 27 secondary features of bathymetry and eight features of image objects. The list of all extracted features (predictor variables) with appropriate references is provided in Table 1. Features 1–3 from this list represent primary datasets from hydroacoustic measurements. Predictors 4–10 were generated in ArcGIS 10.8 software (manufactured by Environmental Systems Research Institute (ESRI), 380 New York Street, Redlands, CA 92373, USA), utilising the Benthic Terrain Modeler (BTM) 3.0 Toolbox (Walbridge et al., 2018). Surface Area to Planar Area (SAPA) represents rugosity, calculated in 3 × 3 neighborhood by division of triangulated raster by two-dimensional pixel area (Jenness, 2004). The slope is the measure of maximum change in depth value (in degrees) regarding the 3 × 3 neighborhood of a pixel. Whereas aspect identifies the surface compass direction in degrees, northness represents the cosine function of the aspect (Burrough and McDonell, 1998). Curvature can be expressed as a slope of a slope. While profile curvature was calculated parallelly to the slope, planar curvature is evaluated perpendicularly to the slope (Zevenbergen and Thorne, 1987).

Features 11–30 were generated in SAGA (System for Automated Geoscientific Analyses) 7.9.0 GIS open-source software (Conrad et al., 2015). The local curvature can be expressed as a sum of the tangents of a pixel slope gradients to its neighbor pixels (Zevenbergen and Thorne, 1987). Curvature classification is a geomorphometric classification based on profile and planar curvatures described in MacMillan and Shary (2009). The upslope curvature was estimated as the distance and flow proportional weighted average local curvature over an upslope of a pixel contributing region after the multiple flow direction algorithm described in Freeman (1991). Similarly, downslope curvature can be expressed as the sum of all downslope connected pixels. Local downslope or upslope curvatures were calculated similarly, considering only neighboring pixels (Freeman, 1991). Cross-sectional curvature can be defined by intersection with the plane of the slope and perpendicular aspect direction, longitudinal curvature represents an intersection of the plane of the slope with aspect direction, following Wood (1996). Maximum and minimum curvatures are the appropriate measures of curvature in any plane. The morphometric features, proposed by Wood (1996), utilise slope and different curvatures to define six different classes of a surface: peak, ridge, pass, plane, channel, and pit. Fuzzy Landform Element Classification (FLEC) is another algorithm utilising geometrical properties of slope and curvature to determine a fuzzy classification of geomorphometric forms (Schmidt and Hewitt, 2004). Multiresolution Index of Valley Bottom Flatness (MRVBF) exploits the inverse of a slope and hierarchy of elevation regarding a circular neighboring area to identify valleys bottoms, Multiresolution Index of the Ridge Top Flatness (MRRTF) is calculated in a very similar way but utilised to find tops of the ridges (Gallant and Dowling, 2003). Vertical Ruggedness Measure (VRM) is a measure of rugosity, calculated based on Sappington et al. (2007). Terrain Surface Classification Landforms, proposed by Iwahashi and Pike (2007), is an unsupervised classification algorithm developed based on slope gradient, local convexity and surface texture. Terrain Surface Classification Convexity is one of the classification criterion used for the calculation of the previous feature. Geomorphons represent landforms extracted from DEM using a machine vision approach, following Jasiewicz and Stepinski (2013). The Topographic Position Index (TPI) working principle is to compare the elevation of each pixel in a DEM to the mean elevation around that pixel, allowing to find ridges, valleys, and flat zones. Terrain Ruggedness Index (TRI) is another measure of topographic heterogeneity, calculated as a sum change in elevation between the pixel and the direct neighboring pixels, described in details in Riley et al. (1999).

Predictors 31–38 were calculated in eCognition software and are related to the shape properties of image objects. Whereas Length/Width can be described as length to width ratio from the bounding box of the image object, Asymmetry was calculated based on the length of an image object based on its regular polygon concerning the surrounding ellipse. While the Density feature describes the distribution of pixels forming an image object, Roundness evaluates the similarity of an image object to an ellipse. Rectangular Fit measured the resemblance of an image object to a rectangle of known proportions. The ratio of the image object's length and width to its area can be described as

Table 1
List of all features extracted in this study with relevant references. 1–3: primary features; 4–30: geomorphometric features; 31–38: object-based features. Y-Yes, N-No.

ID	Feature	Reference	Correlated (Y/N)
1	MBES bathymetry	–	N
2	MBES BBS	–	N
3	SSS image (RGB)	–	R-N; G/B-Y
4	Surface Area to Planar Area (SAPA)	Jenness (2004)	Y
5	Slope	Burrough and McDonell (1998)	Y
6	Aspect	Burrough and McDonell (1998)	Y
7	Northness	Burrough and McDonell (1998)	N
8	Curvature	Zevenbergen and Thorne (1987)	N
9	Profile curvature	Zevenbergen and Thorne (1987)	N
10	Planar curvature	Zevenbergen and Thorne (1987)	N
11	Local curvature	Zevenbergen and Thorne (1987)	Y
12	Curvature classification	MacMillan and Shary (2009)	N
13	Upslope curvature	Freeman (1991)	Y
14	Downslope curvature	Freeman (1991)	N
15	Local Upslope curvature	Freeman (1991)	Y
16	Local Downslope curvature	Freeman (1991)	Y
17	Cross-sectional curvature	Wood (1996)	N
18	Longitudinal curvature	Wood (1996)	Y
19	Maximum curvature	Wood (1996)	Y
20	Minimum curvature	Wood (1996)	Y
21	Morphometric features	Wood (1996)	N
22	Fuzzy Landform Element Classification (FLEC)	Schmidt and Hewitt (2004)	N
23	Multiresolution Index of Valley Bottom Flatness (MRVBF)	Gallant and Dowling (2003)	N
24	Multiresolution Index of the Ridge Top Flatness (MRRTF)	Gallant and Dowling (2003)	N
25	Vector Ruggedness Measure (VRM)	Sappington et al. (2007)	Y
26	Terrain Surface Classification Landforms	Iwahashi and Pike (2007)	N
27	Terrain Surface Classification Convexity	Iwahashi and Pike (2007)	N
28	Geomorphons	Jasiewicz and Stepinski (2013)	N
29	Topographic Position Index (TPI)	Guisan et al. (1999)	Y
30	Terrain Ruggedness Index (TRI)	Riley et al. (1999)	Y
31	Length/Width	Trimble (2014)	N
32	Asymmetry	Trimble (2014)	Y
33	Density	Trimble (2014)	N
34	Roundness	Trimble (2014)	N
35	Rectangular Fit	Trimble (2014)	Y
36	Compactness	Trimble (2014)	Y
37	Elliptic Fit	Trimble (2014)	Y
38	Shape Index	Trimble (2014)	Y

Compactness. Whereas similarity of an image object to an ellipse of known size and shape was calculated using Elliptic Fit, Shape Index informs about the smoothness of the image object border. All used object-based features were described in detail in eCognition's Reference Book (Trimble, 2014).

2.4.4. Feature selection

All attributes from Table 1 were treated by cross-correlation analysis in R software to find and exclude highly correlated features (>0.75 of Pearson's correlation). Then, we computed the Boruta feature selection algorithm (Kursa and Rudnicki, 2016) on uncorrelated part of secondary features (marked 'N' in Table 1). The working principle of the Boruta feature selection algorithm is to find all relevant predictor variables based on shifting with artificial (shadow) attributes generated during multiple iterations in a process that comes from the Random Forest classifier. Boruta outputs a list of the most important features with a measure of their importance (*Z*-Score) (Kursa, 2016).

2.4.5. Supervised classification

The features selected as significant in the feature selection algorithm were utilised as input predictor variables for supervised classifications of image objects. Because each supervised classifier has its strengths and weakness, following recommendations of Lu and Weng (2007), we tested four types of supervised classifiers: Classification and Regression Trees (CART), K-Nearest Neighbor (KNN), Support Vector Machine (SVM), and Random Forest (RF). The summary working principles of these classifiers are as following. CART, developed by Breiman et al. (1984), classifies a dataset based on the decision trees approach. KNN is a simple classifier matching a defined number of nearest neighbors to separate image objects, as described in Bremner et al. (2005). SVM tries to find a perfect hyperplane to classify the dataset in multidimensional space (Cortes and Vapnik, 1995). RF, proposed by Breiman (2001), is the extension of the decision trees approach for multiple trees from which it selects the best solution for classification.

2.4.6. Generalisation of outputs

According to the preliminary requirements of the Polish Chief Inspectorate of Environmental Protection, the planned benthic habitat maps for the Polish waters should be delivered in maps sheets with the most accurate scale of 1:25,000. In this paper, we proposed a mapping generalisation approach tailored to this requirement. A general rule of thumb is that the areas on a map smaller than two by 2 mm are treated by cartographers as the limit of error and can be ignored. Therefore, we generalized the classification outputs to exclude distinct habitat areas of negligible size of 0.002 × 0.002 m (on a map), with respect to scale 1:25,000. Moreover, we made a generalisation comparison with the two more accurate scales: 1:5000 and 1:10,000. After considering the resolution of spatial datasets, the generalisation was made for areas lower than 100 m^2, 400 m^2, and 2500 m^2, respectively. The generalisation was performed in ArcGIS software using Eliminate Polygon Part tool included in the Data Management toolbox.

2.4.7. Accuracy assessment

We calculated accuracy for all classification results, including error matrix and accuracy assessment statistics based on the separate validation subsets of ground-truth samples (Foody, 2002). The applied approach includes calculation of statistics, like user's (Story and Congalton, 1986) and producer's accuracy (Congalton, 1991), and overall accuracy. User's accuracy is measure from the perspective of a map user. It shows how often the class on the map will occur on the real field. The producer's accuracy estimates the accuracy from the perspective of the map maker. It measures how often the real habitat type is showed in the classified map. Overall accuracy is the basic estimate providing the proportion of all reference points that were classified correctly.

The error matrices and accuracy assessment statistics of the same origin were calculated to qualitatively compare the supervised classification results with the manual classification of benthic habitats. A compliance with manual classification was calculated using Tabulate Area tool in the Spatial Analyst toolbox included in ArcGIS. The tool computed cross-tabulated areas between two spatial datasets and outputs a table that was a basis for the error matrix. All results of compliance with the manual classification were provided as percentage values of tabulated areas.

3. Results

3.1. Feature selection

The last column in Table 1 shows that 20 of 40 predictor variables were correlated, so they were removed to avoid overfitting. The result of the Boruta feature selection algorithm provided in Fig. 2 allowed us to evaluate the importance of all extracted features. It shows that 19 of 20 uncorrelated predictor variables were relevant for classification. It is worth noting that the two attributes, Fuzzy Landform Element Classification and Multiresolution Index of the Valley Bottom Flatness, have higher significance than MBES bathymetry. The following two secondary features: Multiresolution Index of the Ridge Top Flatness and Downslope curvature, were more important than SSS image and BBS primary hydroacoustic datasets. In addition, the following seven attributes have formed a group of features with similar relevance as SSS image and BBS. The least important features include three bathymetric and two object-based attributes, of which the last-mentioned were the only object-based features selected in this study.

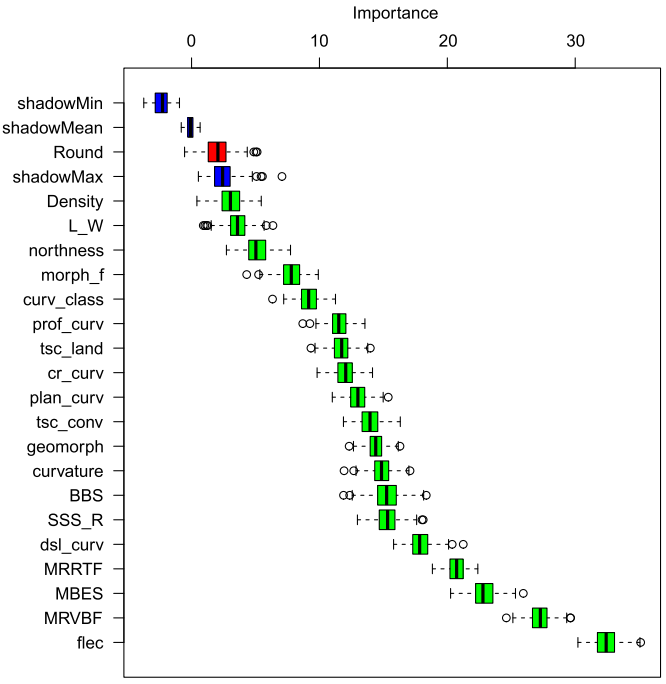

Fig. 2. Result of the Boruta feature selection algorithm (green boxplots—important features; red boxplot—unimportant feature; blue boxplots—shadow variables). The X-axis represents the importance measure of the feature selection algorithm. Used abbreviations: Round—Roundness; L_W—Length/Width; morph_f—Morphometric features; curv_class—Curvature classification; prof_curv—Profile curvature; tsc_land—Terrain Surface Classification Landforms; cr_curv—Cross-sectional curvature; plan_curv—Planar curvature; tsc_conv—Terrain Surface Classification Convexity; geomorph—Geomorphons; SSS_R—Red component of SSS image; dsl_curv—Downslope curvature; MRRTF—Multiresolution Index of the Ridge Top Flatness; MRVBF—Multiresolution Index of the Ridge Top Flatness; flec—Fuzzy Landform Element Classification.

3.2. Benthic habitat mapping

Once developed, the automatic workflow of segmentation classification required approximately 4–5 h to complete multiresolution segmentation and approximately 0.5–1 h to complete the supervised classification process (including all classifiers).

The results of supervised classification and generalized results compared with hydroacoustic datasets and the manual classification of benthic habitats were provided in Figs. 3–10. Each figure consisted of panels, from which the first columns represent hydroacoustic datasets (in the order of MBES bathymetry, BBS, and SSS image) and results of manual classification. The following columns provide the results of supervised classifications in the order of CART, KNN, SVM, RF. The last columns illustrate the generalisation results of areas lower than 2500 m^2 for the following classifiers: CART, KNN, SVM, and RF. The following subchapters describe the geomorphologic details of all study sites, including results of manual classification, then the supervised classification results.

3.2.1. Study site A

Fig. 3 corresponds to the occurrence of the A study site (Fig. 1A). This region has a predominance of glacial relief elements with depths of 13.5–26.9 m b.s.l. The elevations of glacial forms with erosion pavement on the surface are visible Additionally, an elongated hillock of the N-S axis (probable esker) is visible in the central part of the map. A hillock of similar genesis, also with the N-S orientation of the main axis, is located in the southeastern part of the site. The seabed surrounding the hills is flat. Whereas the bottom is sandy on the western side of the meridionally aligned hillock, on the east side, it comprises cohesive sediments with cobbles, individual boulders on the surface, and thin, discontinuous patches of the sandy cover. In the northwestern part of the study site, single irregular, low hills with erosive pavements are visible on the surface.

3.2.2. Study site B

The site consists of the seafloor with a predominance of glacial relief elements with depths 14.9–28.0 m b.s.l. (Fig. 4, Fig. 1B). There are visible hills of glacial formations. In the vicinity of the formations, the bottom is flat, with a discontinuous sand layer. Moreover, sections of the bottom with texture indicative of gravel accumulation are visible.

3.2.3. Study site C

The site represents a rough bottom surface with depths 15.8–19.4 m b.s.l. (Fig. 5). The western part of the study site is an area of the seabed with considerable roughness resulting from outcrops of tills and accumulations of coarse sediments and single boulders on the surface. The eastern part is mainly flat, smooth, with a sandy cover of fine and medium sands.

3.2.4. Study site D

The seabed is flat with single rises and depths of 18.5–23.4 m below sea level. Height of the hills is 2–3 m above the surrounding surface. The seabed is considerably rough, mainly composed of sandy and gravelly sediments with isolated boulders. The majority of the bottom is classified as a mosaic bottom, without clear homogeneous accumulations of sediments such as gravel or sand (Fig. 6J). However, such deposits are visible in the eastern part of the study site - sandy accumulations and two small areas of gravel accumulations.

3.2.5. Study site E

The study site comprises of flat bottom with single hills of glacial origin with erosive pavements on the surface (Fig. 7). The site has depth of 19.4–25.3 m below sea level with elevations up to 3–4 m above the surrounding bottom surface. The ridges of the hills are slightly undulating. There are visible patches and strips of the sand moving along the bottom with NW-SE direction. More significant accumulations of sand were observed near the hills—the remaining seabed surface is composed of glacial deposits with erosive pavements on the surface.

3.2.6. Study site F

The study area has a distinct glacial relief (Fig. 8) and depths of 22.5–24.7 m b.s.l. There are visible series of regular till hills with gravel and stone cover in their ridge part. The hills have the form of slightly curved, long (2–3 km), not high (0.5–1.0 m) arcs with the general NW-SE course. The arcs are curved in the SW direction. The distance between the ridges of the hills ranges from about 150 to 350 m (Fig. 8J). The hills were recognized as hills of the De Geer moraine (Blake, 2000; Kotilainen et al., 2012; Todd, 2016). Sand accumulations (recent marine sand) are visible on the hills' SW (distal) side.

3.2.7. Study site G

The area has a distinct glacial relief (Fig. 9) with depths of 11.5–22.2 m b.s.l. In the southern part of the study site, there is an outcrop of older glacial sediments in the form of a long ridge. The course of the ridge is approximately WSW-ENE. The ridge is up to 3–4 m above the surrounding bottom surface. The rest of the study site shows irregular hummocky moraine hills with a slightly undulating ridge line with erosive pavements on the surface. The hills are up to 5.5 m above the surface of the surrounding bottom. Locally, the seabed is covered by a thin, discontinuous layer of recent marine sands, in the form of ripple marks moving along the hard bottom (till substrate), or patches with a flat surface.

3.2.8. Study site H

The area is located in the southern part of the Slupsk Bank (Fig. 1H). It covers a fragment of the seabed with depths from 19.0 to 32.6 m b.s.l. The site comprises a gently sloping seabed surface, in southerly and south-westerly directions, modelled by recent marine processes. The bottom surface is composed of marine sands, moved mainly in a southerly direction. The depth of the seabed washouts is up to approximately 0.5 m (Fig. 10A). The seabed has mosaic character within the seabed washouts with visible ripple marks, patches and strips of sands, parts with exposed surfaces of flat, sandy, and sandy-silty, locally till seabed.

3.2.9. Supervised classification results

The maps provided in Figs. 3–10 show a good performance of supervised classifiers compared to manual separations of benthic habitats. In most cases, the main separations were extracted appropriately (see Figs. 4, 8, 10). In contrast, all automatic classification results in the G study area (Fig. 9) show some bias towards the overestimation of A5.1 habitat class. Qualitative assessment of supervised classifiers enables to state that performance of the classifiers increases from the CART, through KNN and SVM, to RF. Moreover, the generalized outcomes provided in the last columns of Figs. 3–10 are slightly better compared to manual classification than the raw automatic classification results (middle columns). Therefore, typically, the best classification results are located in panels L and/or I of Figs. 3–10.

Because image objects were generated based on MBES and SSS datasets, all results showed some artifacts, which are mainly the remains of the nadir (dead zone) effect. They are visible mainly as linear structures in Figs. 6–9, affecting the shapes of image objects. The generalisation allowed removal majority of artifacts, but some of them still exist. Besides, it is worth noting that shapes of automatic separations of benthic habitats are more detailed than shapes of manual classification, which are much more smooth.

A matter of particular interest is the occurrence of distinct classes of benthic habitats in automated classification results that were not delineated in manual maps. Some of them can be reasonably found in MBES, BBS, and SSS images but were not noticed in manual maps. A clear example is visible in, e.g., A5.2 class occurrence in the middle of the study site in Fig. 3.

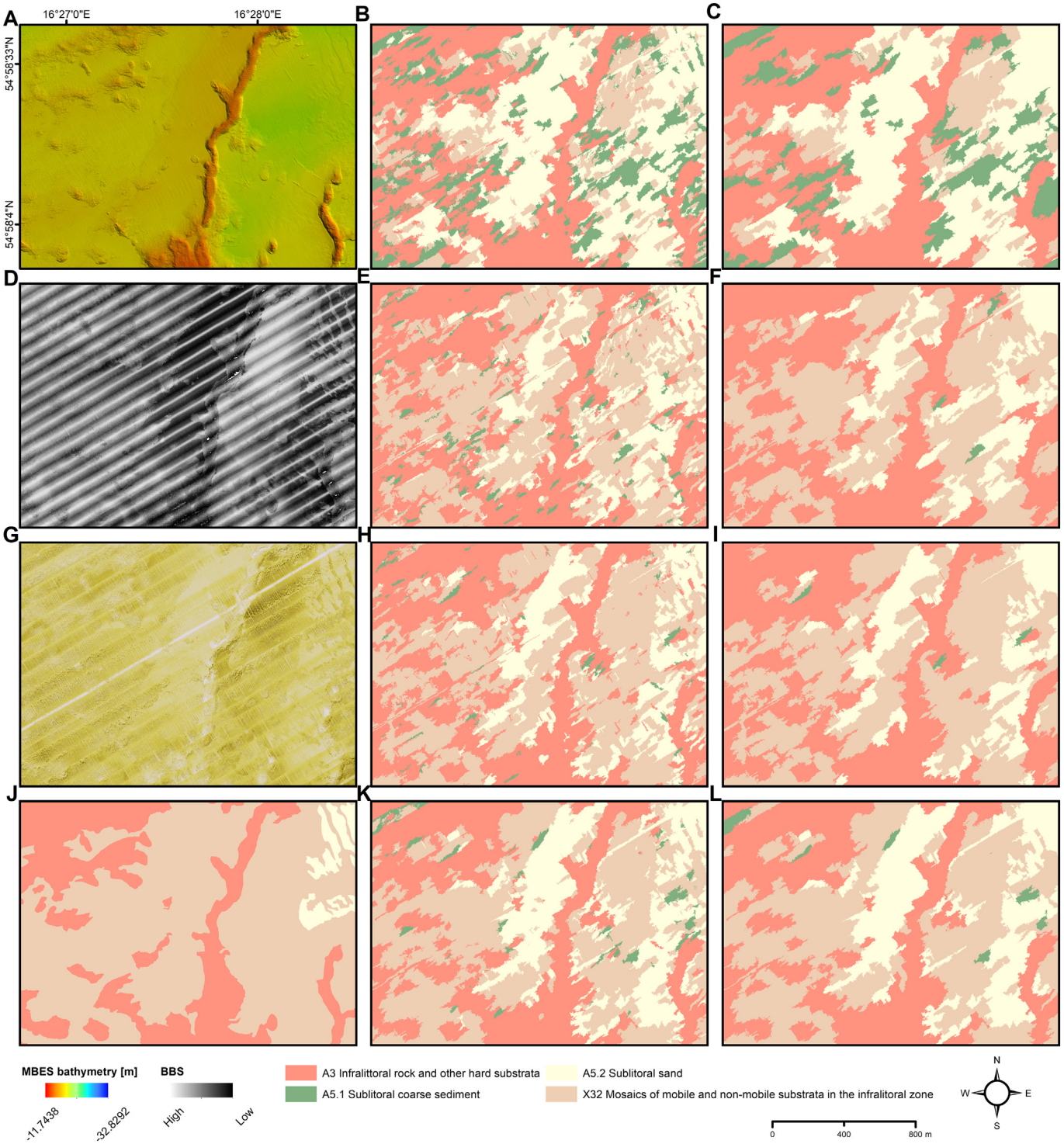

Fig. 3. Hydroacoustic and benthic habitat mapping results for the A study site from Fig. 1: (a) High-resolution bathymetry; (b) CART classification; (c) Generalized CART classification; (d) BBS; (e) KNN classification; (f) Generalized KNN classification; (g) SSS image of the seabed; (h) SVM classification; (i) Generalized SVM classification; (j) Manual benthic habitat classification; (k) RF classification; (l) Generalized RF classification.

3.3. Accuracy assessment

The accuracy assessment results for all supervised classifiers and generalized maps were provided in Table 2. The table cells of error matrices were colored in a white-green scale, showing the most intense green color for the highest accuracy records. The overall accuracy statistics were colored similarly in a white-red scale. The outcomes showed that the best performance was noticed in the Random Forest classifier after generalisation with an overall accuracy of 83%. Compared with the raw automatic classification result, the generalisation improved overall accuracy by 2% in this scenario. Whereas the other scenarios had slightly lower performances, the generalisation allowed to increase the accuracy of the KNN classifier markedly. The lowest accuracy was observed in the CART supervised classifier, which was 9–10% lower than in the RF scenario.

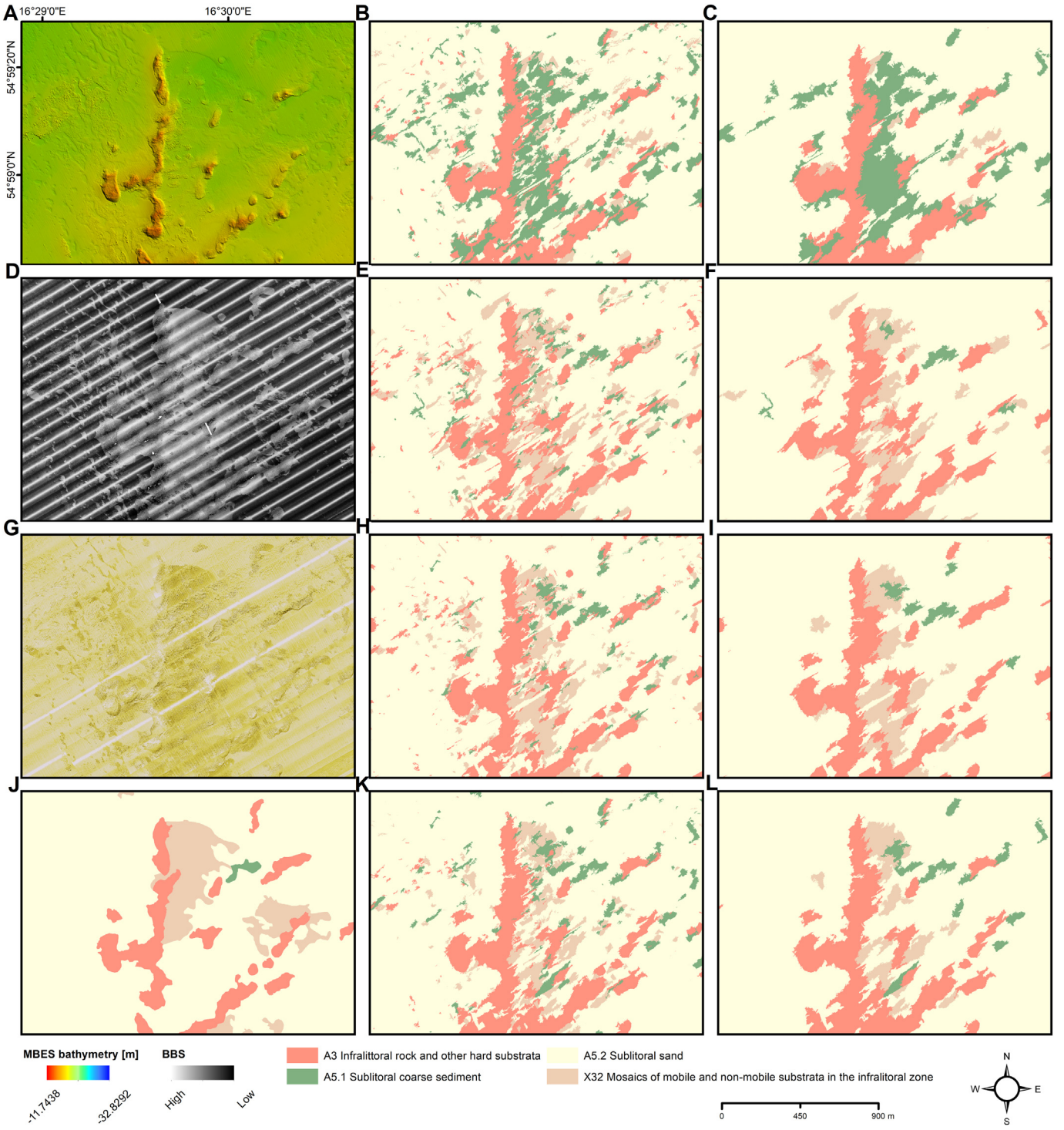

Fig. 4. Hydroacoustic and benthic habitat mapping results for the B study site from Fig. 1: (a) High-resolution bathymetry; (b) CART classification; (c) Generalized CART classification; (d) BBS; (e) KNN classification; (f) Generalized KNN classification; (g) SSS image of the seabed; (h) SVM classification; (i) Generalized SVM classification; (j) Manual benthic habitat classification; (k) RF classification; (l) Generalized RF classification.

The following Table 3 provided results of areal compliance of automatic outputs with manual classification. Similarly, like in the previous table, we marked accuracy assessment statistics in a white-red color scale, where the most intense red shows the highest record. Undoubtedly, Random Forest supervised classifier reached the best results in comparison with manual classification. Furthermore, generalisation allowed to boost SVM scores almost to the RF level. The worst classifier (CART) global scores were over 10% less than in the best classifier. It is worth noting that the User's and Producer's statistics are roughly evenly distributed between classes in the case of RF, whereby the distribution decreased towards classifiers with worse performance (CART).

4. Discussion

4.1. Reference to the main research objectives

In this study, the following actions were performed to answer the research questions stated in the Introduction: (a) development of the

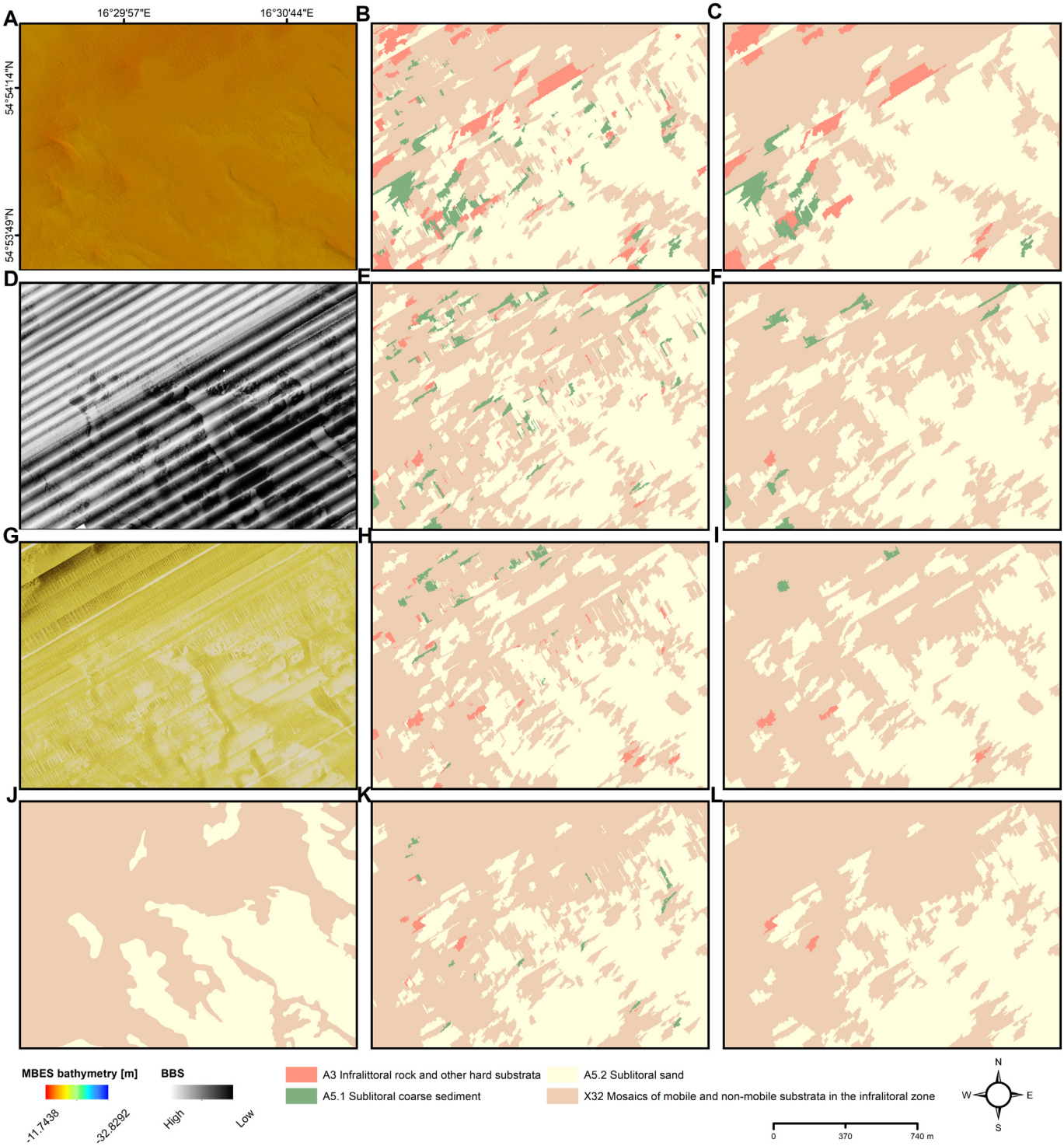

Fig. 5. Hydroacoustic and benthic habitat mapping results for the C study site from Fig. 1: (a) High-resolution bathymetry; (b) CART classification; (c) Generalized CART classification; (d) BBS; (e) KNN classification; (f) Generalized KNN classification; (g) SSS image of the seabed; (h) SVM classification; (i) Generalized SVM classification; (j) Manual benthic habitat classification; (k) RF classification; (l) Generalized RF classification.

objective, repeatable, transparent and quick automatic workflow based on object-based image analysis; (b) selection of relevant predictor variables and comparison of multiple classification models; (c) qualitative comparison of the classification performance vs manual maps for different study areas; (d) quantitative comparison of supervised classification models with the generalized classification maps. The following paragraphs contain a detailed discussion of the results, their interpretation, implications of this study and future research directions.

4.2. Interpretation of results

The feature selection results provided in the previous section suggests high relevance of the four geomorphometric predictor

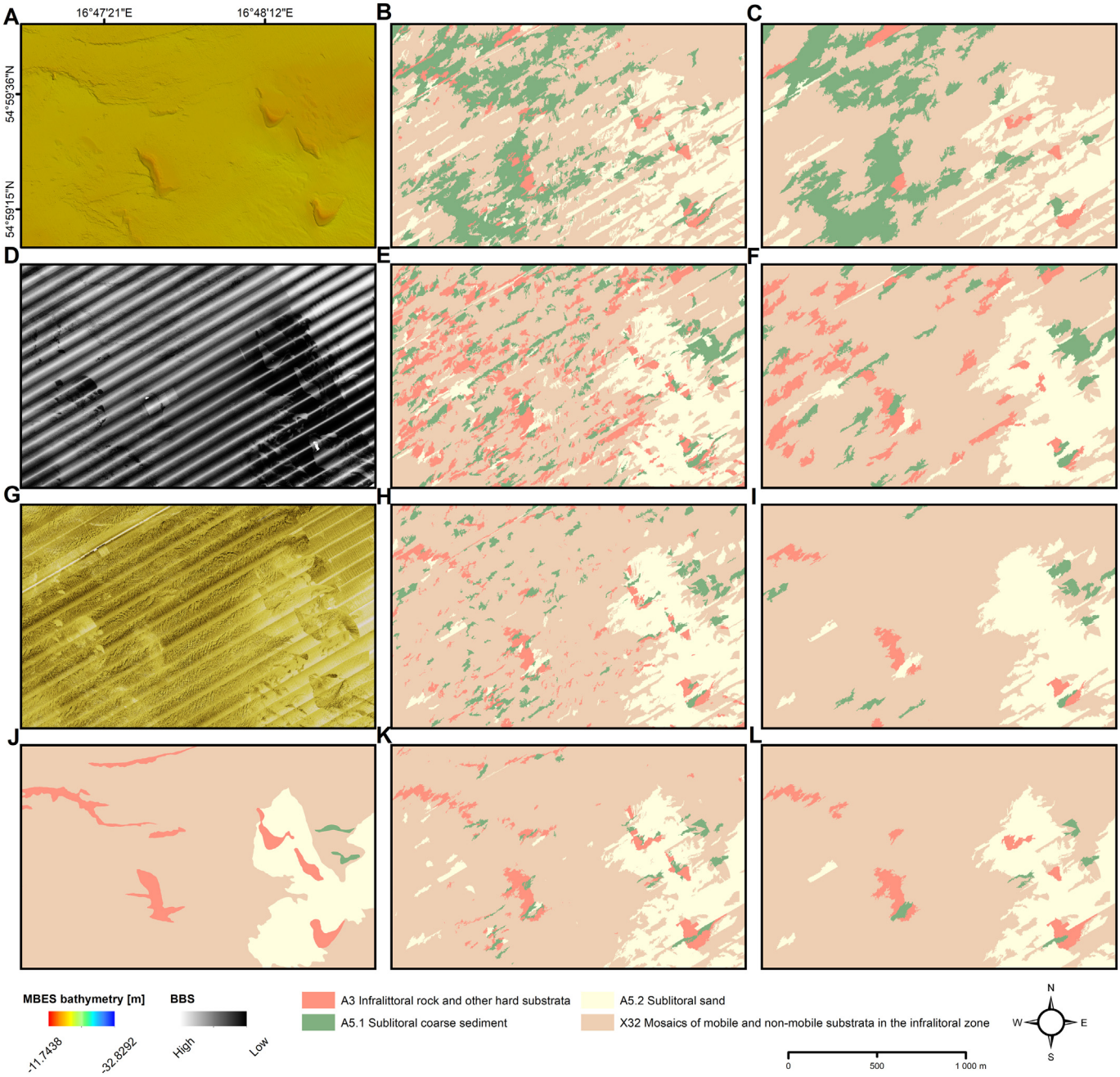

Fig. 6. Hydroacoustic and benthic habitat mapping results for the D study site from Fig. 1: (a) High-resolution bathymetry; (b) CART classification; (c) Generalized CART classification; (d) BBS; (e) KNN classification; (f) Generalized KNN classification; (g) SSS image of the seabed; (h) SVM classification; (i) Generalized SVM classification; (j) Manual benthic habitat classification; (k) RF classification; (l) Generalized RF classification.

variables: Fuzzy Landform Element Classification and Multiresolution Index of the Valley Bottom Flatness, Multiresolution Index of the Ridge Top Flatness and Downslope curvature. Whereas the mean importance *Z*-score of the first two was approximately 33 and 27, MBES bathymetry had 23. Additionally, the following features' relevance measure was around 21 and 18, before the SSS image having 15 Z-score. These novel results have shown a significant relevance of the mentioned geomorphometric parameters that can noticeably improve the classification performance of benthic habitats.

The total time needed to perform the methodological procedure developed in this article was finished after a few hours of calculation on consumer mid-range mobile workstation. In comparison, the detailed manual determination of benthic habitats required a much longer time to be finished. It is important to remember that a well-executed manual classification should ideally be performed by a single interpreter. Thus, automatic approach can significantly support manual classification by its repeatability and objectivity, which is unquestionable for benthic habitat mapping of extensive areas.

Qualitative assessment of supervised classification results indicated that RF had the highest performance in determining benthic habitats. Adapting the scale from Landis and Koch (1977) to our overall accuracy results can be interpreted as an almost perfect agreement (0.81–1.00). The generalisation approach presented in this study slightly increased the performances of all classification models. Moreover, the generalized maps lacked some errors that occurred due to the small sizes of image

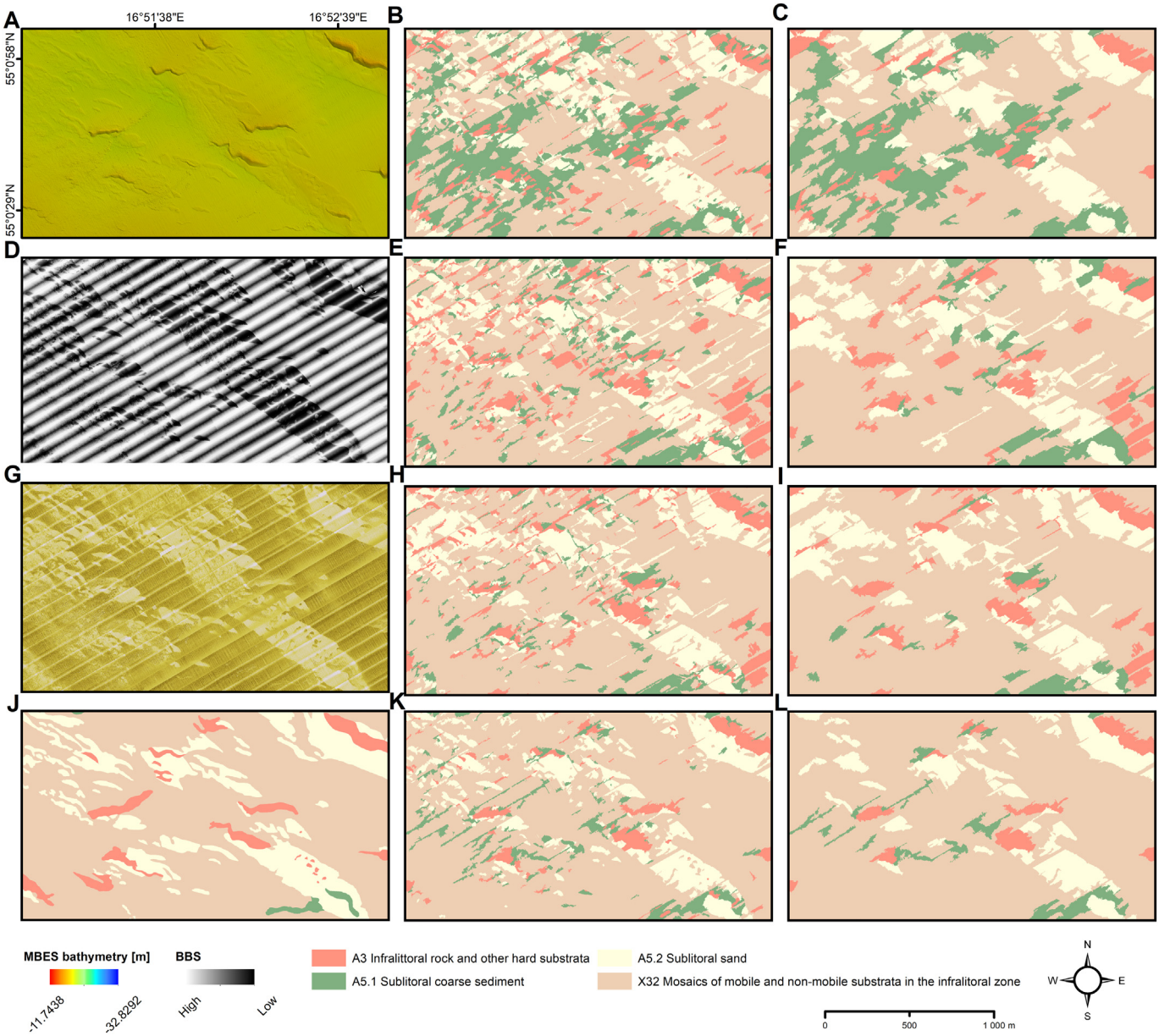

Fig. 7. Hydroacoustic and benthic habitat mapping results for the E study site from Fig. 1: (a) High-resolution bathymetry; (b) CART classification; (c) Generalized CART classification; (d) BBS; (e) KNN classification; (f) Generalized KNN classification; (g) SSS image of the seabed; (h) SVM classification; (i) Generalized SVM classification; (j) Manual benthic habitat classification; (k) RF classification; (l) Generalized RF classification.

objects and artifacts resulting from the processing of hydroacoustic datasets.

4.2.1. Geomorphological interpretation and discussion

The results of automatic analyses were compared with the outputs of manual classifications. Manually classified maps had a clearly lower degree of details than maps created in automatic classification. We checked the possibility of introducing areas separated by automatic classifications but not introduced during manual classifications. The analysis showed that such an interpretation is possible and correct. Some separations were not introduced in manual classifications due to doubts that appeared during the interpretation processes. Classification doubts arose when the distinguished areas were small and could be classified both as, e.g. (generalized) mosaic bottom and individual small areas of coarse/hard bottom within the mosaic bottom.

The well-chosen segmentation scale of the automatic analysis allowed to indicate additional bottom parts of a different character (e.g., study site B and G - additional coarse bottom fragments; study site C - additional hard bottom fragments). The smallest differences between manual and automatic interpretation results were related to the extent of sandy bottom and distinct ridges within the hard bottom. The largest differences were detected for flat bottom areas with a wide variety of bottom sediments (see, e.g., Diesing et al., 2020). The general delineation "mosaic bottom" was more frequently introduced during manual analysis within such seabed fragments. In these same areas, automatic analysis introduced additional, more detailed separations due to the more detailed investigations. Due to their small areas, some of these separations were removed according to the assumed generalisation approach.

Manual classification of benthic habitats separated boundaries between particular types of classes with generalisation resulting from the scale of the map on which they were interpreted. During the automatic classification, these boundaries retain the character of the full resolution of the source data, hence their more varied shape.

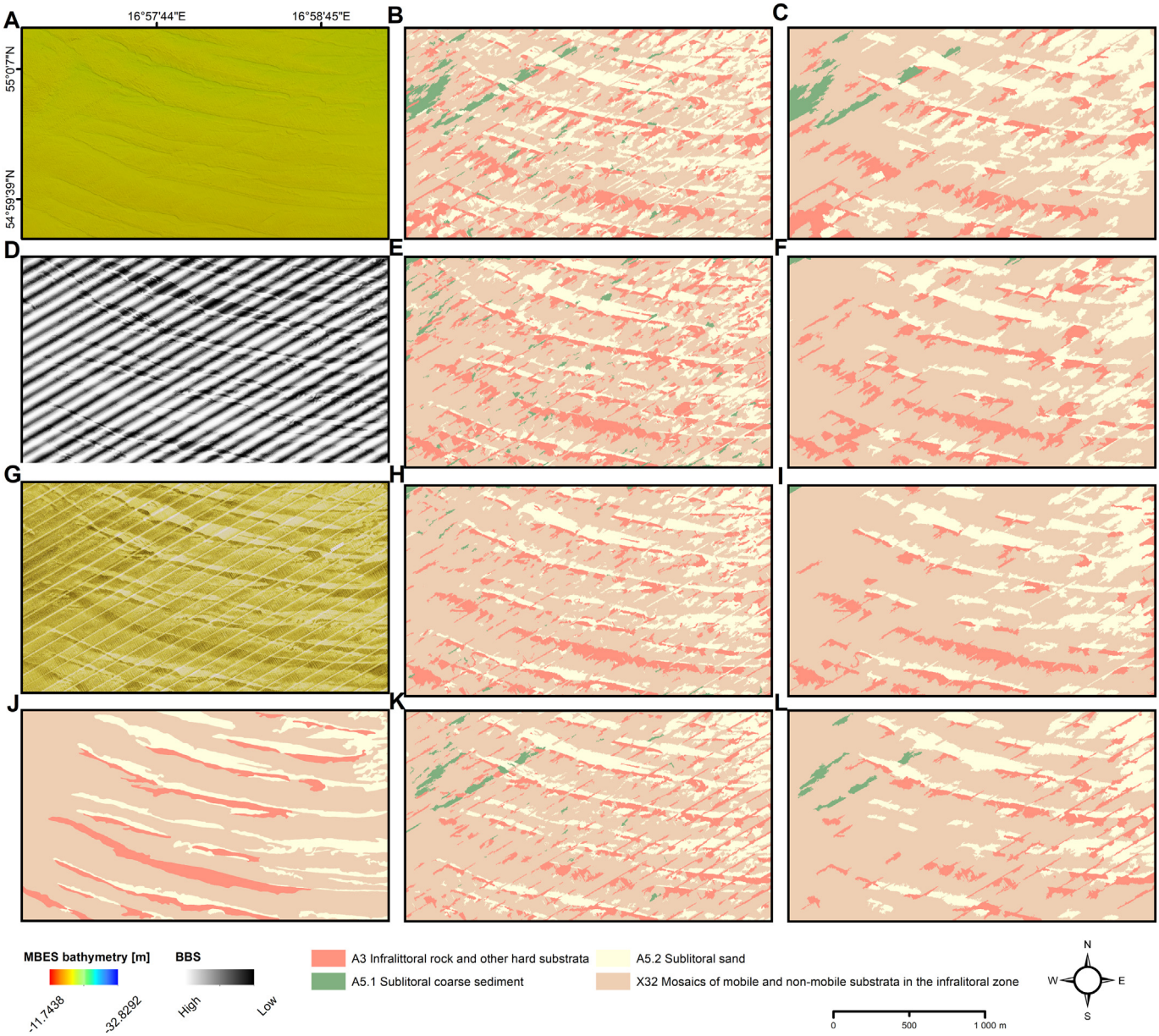

Fig. 8. Hydroacoustic and benthic habitat mapping results for the F study site from Fig. 1: (a) High-resolution bathymetry; (b) CART classification; (c) Generalized CART classification; (d) BBS; (e) KNN classification; (f) Generalized KNN classification; (g) SSS image of the seabed; (h) SVM classification; (i) Generalized SVM classification; (j) Manual benthic habitat classification; (k) RF classification; (l) Generalized RF classification.

The manual classification unintentionally omitted some objects occupying small areas, which corresponded to the assumed minimum area of separations. In addition, during manual classification, artifacts resulting from the processing of bathymetric and sonar data were omitted. Whereas human interpretation of the image allows filtering the erroneous data, some of these artifacts are visible on the automatic benthic habitat maps.

Manual interpretation of the flat seafloor comprises difficulties in interpretation. Especially areas without clear visible morphological boundaries introduce uncertainty in delineating the extent of a given bottom type. This is visible, for example, in areas of a sandy seabed gradually transitioning into, e.g., mosaic bottom. The common interpretation problem in this scenario provides the following question: "is the bottom still sandy or already mosaic at a given location?". Similar uncertainties appeared in areas of a hard bottom with erosive pavements on the surface, comprising the following issue: "Do we still classify the bottom as hard with erosive pavements (including gravel) on the surface, or should we classify this fragment as a coarse bottom?". Such doubts do not exist in the machine learning classification. We checked each study site within this approach and admitted that the proposed automatic separations do not contradict the possible manual interpretation.

Excellent examples of interpretative uncertainty are areas with thin sand cover, located in, e.g., study site C. In this scenario, even a small change in depth and seafloor roughness was an indicator of sand extent. The other example of an accurate automatic interpretation were areas with minimally different seafloor roughness indicating the presence of coarse-grained material (gravel), not marked during manual interpretation (study sites D and E). Whereas manually, these areas were indicated as hard bottom, the automatic classification result provided additional regions of the coarse-grained bottom, highlighted within the hard bottom.

The De Geer moraine area (located in the study site F) is an excellent example of a surface with minor denivelations and low artifacts from the bathymetric measurements. In the manual interpretation, the artifacts were omitted, and the ridges of the De Geer moraines were highlighted. In contrast, the automatic interpretation produced an

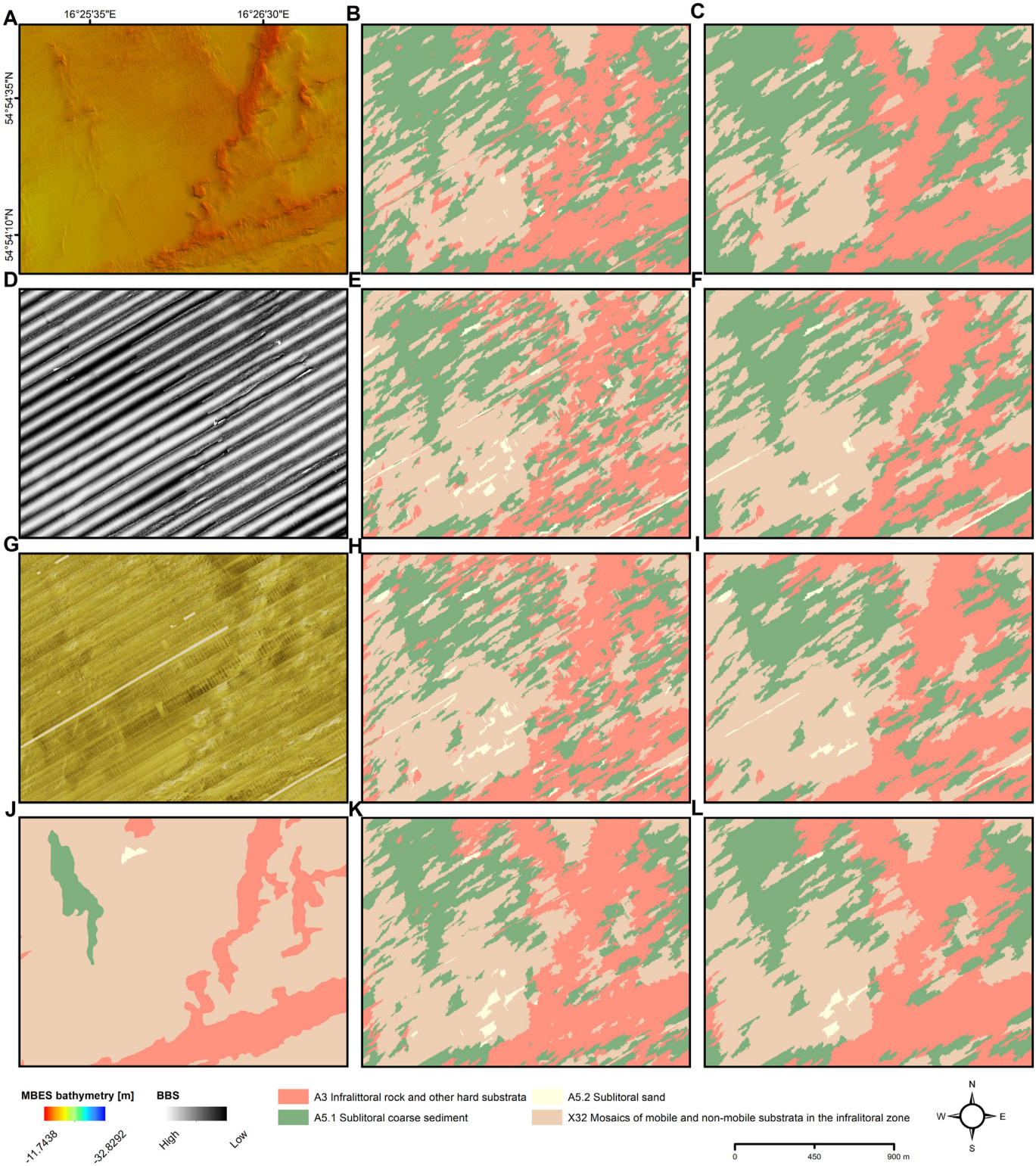

Fig. 9. Hydroacoustic and benthic habitat mapping results for the G study site from Fig. 1: (a) High-resolution bathymetry; (b) CART classification; (c) Generalized CART classification; (d) BBS; (e) KNN classification; (f) Generalized KNN classification; (g) SSS image of the seabed; (h) SVM classification; (i) Generalized SVM classification; (j) Manual benthic habitat classification; (k) RF classification; (l) Generalized RF classification.

image with visible noise (artifacts). Nevertheless, the nature of the course of the ridges is correct, and the image was enhanced with the indicated additional fragments of the coarse-grained bottom. Thus, during automatic classification, the seabed image was not overinterpreted, artificially emphasized. However, it is worth noting that such an emphasis may be introduced during manual interpretation. For example, when the form boundaries are very poorly defined in the bottom relief, and the interpreter wants to emphasize and strengthen them to indicate the elements of the bottom relief that are important for the analyses.

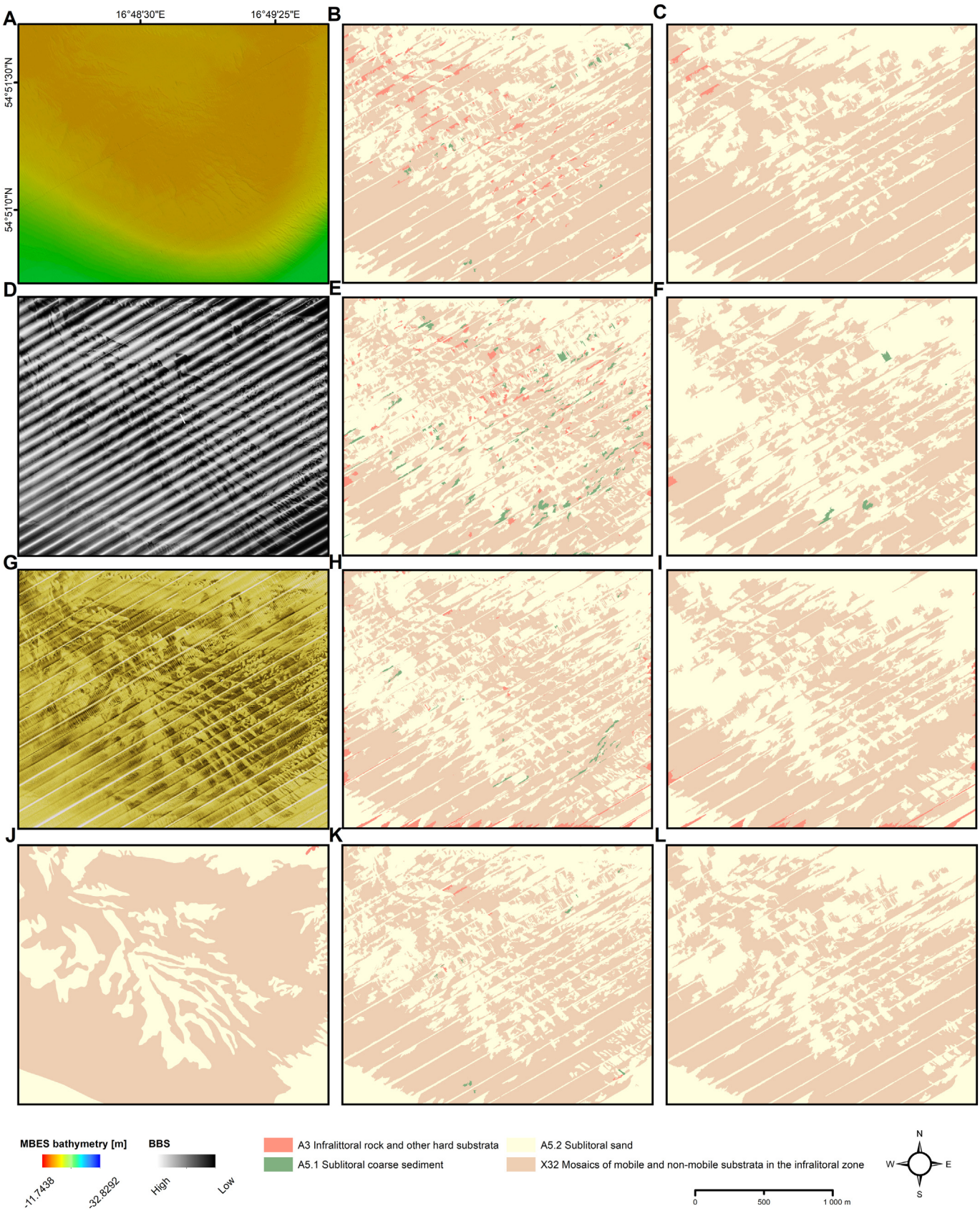

Fig. 10. Hydroacoustic and benthic habitat mapping results for the H study site from Fig. 1: (a) High-resolution bathymetry; (b) CART classification; (c) Generalized CART classification; (d) BBS; (e) KNN classification; (f) Generalized KNN classification; (g) SSS image of the seabed; (h) SVM classification; (i) Generalized SVM classification; (j) Manual benthic habitat classification; (k) RF classification; (l) Generalized RF classification.

Table 2
Error matrices and accuracy assessment statistics for four supervised classifications (top tables) and generalized maps (down tables with 2500 annotation), based on validation ground-truth samples.

CART

Prediction \ Reference	A3	A5.1	A5.2	X32	Sum
A3	103	6	0	14	123
A5.1	29	132	8	21	190
A5.2	4	4	119	36	163
X32	14	8	23	79	124
Sum	150	150	150	150	600
User's	0.84	0.69	0.73	0.64	
Producer's	0.69	0.88	0.79	0.53	
Overall	0.72				

KNN

Prediction \ Reference	A3	A5.1	A5.2	X32	Sum
A3	107	8	8	17	140
A5.1	14	130	2	13	159
A5.2	6	3	124	32	165
X32	23	9	16	88	136
Sum	150	150	150	150	600
User's	0.76	0.82	0.75	0.65	
Producer's	0.71	0.87	0.83	0.59	
Overall	0.75				

SVM

Prediction \ Reference	A3	A5.1	A5.2	X32	Sum
A3	113	17	4	18	152
A5.1	11	113	0	7	131
A5.2	4	5	134	26	169
X32	22	15	12	99	148
Sum	150	150	150	150	600
User's	0.74	0.86	0.79	0.67	
Producer's	0.75	0.75	0.89	0.66	
Overall	0.77				

RF

Prediction \ Reference	A3	A5.1	A5.2	X32	Sum
A3	117	7	2	9	135
A5.1	8	133	3	5	149
A5.2	4	4	133	33	174
X32	21	6	12	103	142
Sum	150	150	150	150	600
User's	0.87	0.89	0.76	0.73	
Producer's	0.78	0.89	0.89	0.69	
Overall	0.81				

CART 2500

Prediction \ Reference	A3	A5.1	A5.2	X32	Sum
A3	100	0	3	14	117
A5.1	28	135	7	19	189
A5.2	6	5	123	39	173
X32	16	10	17	78	121
Sum	150	150	150	150	600
User's	0.85	0.71	0.71	0.64	
Producer's	0.67	0.90	0.82	0.52	
Overall	0.73				

KNN 2500

Prediction \ Reference	A3	A5.1	A5.2	X32	Sum
A3	112	0	6	16	134
A5.1	8	137	0	5	150
A5.2	11	3	126	27	167
X32	19	10	18	102	149
Sum	150	150	150	150	600
User's	0.84	0.91	0.75	0.68	
Producer's	0.75	0.91	0.84	0.68	
Overall	0.80				

SVM 2500

Prediction \ Reference	A3	A5.1	A5.2	X32	Sum
A3	116	0	2	14	132
A5.1	6	127	0	7	140
A5.2	8	7	135	27	177
X32	20	16	13	102	151
Sum	150	150	150	150	600
User's	0.88	0.91	0.76	0.68	
Producer's	0.77	0.85	0.90	0.68	
Overall	0.80				

RF 2500

Prediction \ Reference	A3	A5.1	A5.2	X32	Sum
A3	117	0	4	6	127
A5.1	6	138	0	4	148
A5.2	6	3	134	30	173
X32	21	9	12	110	152
Sum	150	150	150	150	600
User's	0.92	0.93	0.77	0.72	
Producer's	0.78	0.92	0.89	0.73	
Overall	0.83				

The automatic method allowed capturing areas that were misclassified during manual analysis. An example is a fragment of the study site A. The sand accumulation visible on the hill's western side was not indicated in manual interpretation but appeared on automatic classification.

During manual interpretation, an author's understanding of the nature of the bottom is formed. This entails a subjective approach to delineations of habitat classes. Consequently, some elements of the bottom are emphasized. This is not pointed out as an error because any form of interpretation - whether manual or automatic, involves the authorial preparation of interpretive assumptions. However, it is noteworthy that subjectivity will be much more stable in automatic analysis than manual interpretation.

Excellent correlation with the SSS and MBES data is presented in study site H - an area with slight depth variation but with different sediment character of the seabed. The differences between automatic and manual concern the detail of the final image. Automatic classification delineated more clear boundaries, but artifacts are also visible.

A difficulty when interpreting automatic classification is the visible artifacts. An example of such an area is the study site C. Visible within its

Table 3
Compliance with the manual classification of benthic habitats, represented in percentage error matrices and accuracy assessment statistics for four supervised classifications (top tables) and generalized maps (down tables with 2500 annotation).

CART

Prediction \ Reference	A3	A5_1	A5_2	X32	Sum
A3	6.61	1.66	0.38	0.64	9.29
A5.1	0.03	0.61	0.00	0.03	0.67
A5.2	0.87	1.33	19.84	3.94	25.99
X32	5.27	10.62	12.42	35.74	64.06
Sum	12.78	14.23	32.64	40.35	100.00
User's	0.71	0.92	0.76	0.56	
Producer's	0.52	0.04	0.61	0.89	
Overall	0.63				

KNN

Prediction \ Reference	A3	A5_1	A5_2	X32	Sum
A3	6.40	1.08	0.33	1.48	9.29
A5.1	0.03	0.61	0.00	0.03	0.67
A5.2	1.02	0.46	20.35	4.15	25.99
X32	6.91	5.40	11.80	39.94	64.06
Sum	14.36	7.55	32.49	45.60	100.00
User's	0.69	0.92	0.78	0.62	
Producer's	0.45	0.08	0.63	0.88	
Overall	0.67				

SVM

Prediction \ Reference	A3	A5_1	A5_2	X32	Sum
A3	6.99	0.69	0.49	1.13	9.29
A5.1	0.10	0.46	0.00	0.10	0.67
A5.2	0.95	0.15	21.27	3.61	25.99
X32	5.33	3.58	10.47	44.67	64.06
Sum	13.36	4.89	32.23	49.51	100.00
User's	0.75	0.69	0.82	0.70	
Producer's	0.52	0.09	0.66	0.90	
Overall	0.73				

RF

Prediction \ Reference	A3	A5_1	A5_2	X32	Sum
A3	7.32	0.38	0.31	1.28	9.29
A5.1	0.03	0.61	0.00	0.03	0.67
A5.2	0.74	0.26	21.43	3.56	25.99
X32	4.28	3.89	9.09	46.80	64.06
Sum	12.37	5.15	30.82	51.66	100.00
User's	0.79	0.92	0.82	0.73	
Producer's	0.59	0.12	0.70	0.91	
Overall	0.76				

CART 2500

Prediction \ Reference	A3	A5.1	A5.2	X32	Sum
A3	6.58	1.44	0.39	0.79	9.20
A5.1	0.00	0.46	0.02	0.04	0.52
A5.2	0.57	1.32	19.28	4.41	25.59
X32	5.09	10.07	11.95	37.60	64.70
Sum	12.23	13.28	31.64	42.84	100.00
User's	0.72	0.89	0.75	0.58	
Producer's	0.54	0.03	0.61	0.88	
Overall	0.64				

KNN 2500

Prediction \ Reference	A3	A5_1	A5_2	X32	Sum
A3	6.85	0.53	0.46	1.35	9.20
A5.1	0.00	0.48	0.01	0.03	0.52
A5.2	0.75	0.30	20.32	4.21	25.59
X32	5.43	4.20	11.35	43.72	64.70
Sum	13.04	5.50	32.15	49.30	100.00
User's	0.75	0.92	0.79	0.68	
Producer's	0.53	0.09	0.63	0.89	
Overall	0.71				

SVM 2500

Prediction \ Reference	A3	A5_1	A5_2	X32	Sum
A3	7.16	0.33	0.44	1.26	9.20
A5.1	0.00	0.44	0.02	0.06	0.52
A5.2	0.73	0.11	20.85	3.90	25.59
X32	4.54	3.02	9.82	47.32	64.70
Sum	12.44	3.89	31.13	52.54	100.00
User's	0.78	0.85	0.81	0.73	
Producer's	0.58	0.11	0.67	0.90	
Overall	0.76				

RF 2500

Prediction \ Reference	A3	A5_1	A5_2	X32	Sum
A3	6.97	0.40	0.39	1.44	9.20
A5.1	0.00	0.46	0.01	0.04	0.52
A5.2	0.80	0.21	20.65	3.93	25.59
X32	3.92	3.27	8.45	49.07	64.70
Sum	11.69	4.34	29.50	54.47	100.00
User's	0.76	0.89	0.81	0.76	
Producer's	0.60	0.11	0.70	0.90	
Overall	0.77				

boundaries are accumulations of sand with a general NW-SE alignment resulting from the direction of sand movement along the bottom. The automatic interpretation data show interference with the direction of the bathymetric and sonar measurements, e.g., SW-NE. These disturbances disturb the correct image of the sand accumulation system. In such cases, it is necessary to correct the obtained interpretations manually.

A similar difference, resulting from the quality of bathymetric data, concerns the continuity and course of the boundaries of distinguished bottom areas. An example is the forms in the western part of the study site D. These are elevations with a slightly undulating course of the top parts of ridges. The automatic classification fragmented or not distinguished these elevations (see the form in the NW part of the study site) due to their low height and artifacts from acoustic measurements (Fig. 6).

4.3. Implications of this study in relation to other works

Up to our best knowledge, the following predictor variables were not used before in benthic habitat mapping or seafloor characterisation studies: Fuzzy Landform Element Classification, Multiresolution Index of the Valley Bottom Flatness, Multiresolution Index of the Ridge Top Flatness, Terrain Surface Classification Landforms, and Terrain Surface Classification Convexity. Whereas morphometric features predictor variable was previously used for mapping of, e.g., rocky reefs (Lucieer and Pederson, 2008; Zieger et al., 2009), geomorphons or bathymorphons (Masetti et al., 2018) are the features that were utilised several times to perform seafloor classification based on hydroacoustic data (Sowers et al., 2020). In contrast, object-based features, like Length/Width, were previously seldom used to detect underwater archaeological objects based on multibeam echosounder measurements (Janowski et al., 2021). The relevance of some of the secondary features presented in this study shows their high potential for utilisation in further benthic habitat mapping studies. Although most research showing Boruta feature selection results stated primary features of hydroacoustic measurements as the most relevant features (Janowski et al., 2018; Rende et al., 2020), our results show that it is not always the case.

Evaluation of different supervised classifiers is a reasonable way to improve overall mapping result. Therefore, this study is in line with several previous works that tested different supervised classifiers to estimate the model with the best performance (Calvert et al., 2015; Hasan et al., 2012; Ierodiaconou et al., 2018; Montereale Gavazzi et al., 2016). Concerning the other benthic habitat mapping works based on the supervised classification approach, the model performance presented in this work can be assessed as reliable. To compare, the other recent works state the highest overall accuracy of the supervised classifiers in the ranges of 60–70% (Zelada Leon et al., 2020), 70–80% (Goodman et al., 2020; Proudfoot et al., 2020), 80–90% (Jarna et al., 2019; Montereale-Gavazzi et al., 2018; Porskamp et al., 2018; Shang et al., 2021) and 90–100% (Enwright et al., 2019).

Although the main purpose of this study was to conduct seabed classification based on the morphological analysis of the seafloor surface and the building sediments (EUNIS level 3), the method presented in this research works well also for determination of specific benthic communities. Previous attempts of such research were successfully conducted in 2018/2020 in the shallow nearshore parts of the Baltic Sea. They allowed to distinguish more detailed habitats, e.g., red algae based on multibeam echosounder measurements (Janowski et al., 2018; Trzcinska et al., 2020). The main requirements for more detailed classification of benthic habitats include detailed ground-truth sampling annotations and high-resolution hydroacoustic measurements (possibly covering multiple frequencies) (Brown et al., 2019; Gaida et al., 2019).

4.4. Limitations of the study

Although the generalisation removed most of the linear artifacts visible in Figs. 6–9, some still exist. We tested different parameters of multiresolution segmentation on different sets of primary layers to create the most meaningful image objects. The tested parameters included scale from 10 to 2000, shape from 0.1 to 0.9, and compactness from 0.1 to 0.9. The visual assessment of segmentation results indicated that the highest precision of benthic habitat separations was done for scale 150, shape 0.1, and compactness 0.5. Compared with manual maps of benthic habitats, delineation of image objects was much more detailed, in return containing possible linear artifacts from hydroacoustic measurements. This effect was partly eliminated in the generalisation process.

In this study, we designed random ground-truth points to ensure a similar number of points and possibly high statistical significance for each class. Our User's and Producer's statistics have shown that accuracy was uniformly distributed between all classes (Table 2). A large number of samples provided the high statistical significance of the results (Carlotto, 2009). However, it is worth noting that the spatial arrangement of ground-truth points varied depending on the spatial coverage occupied by specific habitats. The example was visible in Fig. 1G, where the restricted area of class A5.1 (compare with Fig. 9J) forced the generation of ground-truth points that were distributed with a higher density than other cases. It seems that a denser distribution of points may have impacted the possible overestimation of class A5.1 in classification results presented in the G study area (Fig. 9). Therefore, we assume that uniform distribution of ground-truth points throughout the whole area could reduce the overestimation of such habitats. In exchange, fewer points for smaller habitats lower the statistical significance of the analysis.

The other issue is related to the training/test ratio used for the automatic classification of the hydroacoustic dataset. Although the common separation ratio used in this research was performed using a simple single split approach (Lyons et al., 2018), some studies suggest testing the other approaches and other separation ratios (Mitchell et al., 2018). Detailed, complete recognition of large seabed areas requires high-resolution hydroacoustic measurements. Among others, to reduce survey costs, usually, data are acquired using a wide spectrum of methods during one survey campaign. These include multibeam echosounder, side-scan sonar as well as seismoacoustic equipment. With appropriately selected parameters of measuring devices we obtain a sufficiently rich dataset that can be used for the analyses presented by us. Processing of hydroacoustic datasets requires software that are usually dedicated to the particular device. Despite collecting an appropriate dataset during one survey, performing this type of research is still expensive. To reduce the costs of research, at the current stage of seabed exploration and mapping, we also use data collected during other surveys, surveys conducted for other purposes (e.g., surveys for offshore wind farms and their offshore infrastructure connection, underwater cables, underwater pipelines, monitoring of seabed conditions). We expect that the use of autonomous measuring devices (unmanned surface vessels / autonomous underwater vehicles) would reduce the costs of such surveys. From the software point of view, we used several different programs for benthic habitat mapping. The two of them are commercial (ArcGIS and eCognition). Being very widely used, ArcGIS is standard commercial software for GIS purposes, and research institutions usually have access to the current program license. eCognition is less commonly used and more expensive, but there exist options for educational or non-commercial use licenses. The other software used (R, SAGA GIS) are open-sourced, as was mentioned in the methodology section.

4.5. Recommendations for future research

Benthic habitat mapping or seafloor characterisation studies based on hydroacoustic measurements usually benefit from various geomorphometric features developed previously for terrain landform studies. Our results suggested a very high relevance of specific geomorphometric features, even higher than the bathymetry itself for classifying benthic habitats. These include Fuzzy Landform Element Classification and Multiresolution Index of the Valley Bottom Flatness

and Multiresolution Index of the Ridge Top Flatness that were not used in this field of study before. Future research may also benefit from other predictor variables that were not used before in benthic habitat mapping and were slightly less relevant than primary features in this study. These include Terrain Surface Classification Landforms and Terrain Surface Classification Convexity. We recommend incorporating and further evaluating their use in other study areas based on hydroacoustic measurements.

5. Conclusions

This study represents the first insight for high-resolution hydroacoustic surveys in the Slupsk Bank Natura 2000 site. The quick and transparent, automatic classification workflow of a single classifier for benthic habitat mapping of eight study sites located within the area was developed. Some of the extracted geomorphometric predictor variables were novel in benthic habitat mapping studies and shown significant importance for the automatic procedure. Comparison of classification results with manual maps demonstrated that Random Forest had the highest performance of four tested supervised classifiers. The generalisation requirement further improved classification performance relevant for benthic habitat mapping of very large spatial areas planned to be performed in the Polish Exclusive Economic Zone. The fundamental discoveries of this research suggest the use of several approaches to improve the accuracy and performance of automatic modeling of benthic habitats. They may be helpful for mapping other extensive areas based on MBES and SSS datasets.

CRediT authorship contribution statement

Conceptualization, L.J., R.W., J.D. and J.G.; methodology, L.J.; software, L.J.; validation, M.W.; formal analysis, L.J.; investigation, L.J., R.W. and J.D.; resources, R.W., J.D. and J.G.; data curation, M.K., K.R., R.W. and J.D.; writing—original draft preparation, L.J.; writing—review and editing, L.J.; visualisation, L.J.; supervision, J.G.; project administration, J.G.; funding acquisition, L.J. All authors have read and agreed to the published version of the manuscript.

Funding

This research was funded from the MEWO company own funds. Side-scan sonar survey was funded by Maritime Office in Slupsk based on the "Development of a draft plan of protection with public consultations for the Slupsk Bank (PLC 990001) Natura 2000 maritime area" Agreement of July 05, 2018, between Maritime Office in Slupsk and Maritime Institute in Gdansk in consortium with MEWO S.A.

Data availability statement

The data that support the findings of this study are available from the corresponding author upon reasonable request.

Declaration of competing interest

The authors declare no conflict of interest.

References

Andrulewicz, E., Kruk-Dowgiallo, L., Osowiecki, A., 2004. Phytobenthos and macrozoobenthos of the Slupsk Bank stony reefs, Baltic Sea. Hydrobiologia 514, 163–170.

Benz, U.C., Hofmann, P., Willhauck, G., Lingenfelder, I., Heynen, M., 2004. Multi-resolution, object-oriented fuzzy analysis of remote sensing data for GIS-ready information. ISPRS J. Photogramm. Remote Sens. 58, 239–258.

Blake, K.P., 2000. Common origin for De geer moraines of variable composition in raudvassdalen, northern Norway. J. Quat. Sci. 15, 633–644.

Bøe, R., Bjarnadóttir, L.R., Elvenes, S., Dolan, M., Bellec, V., Thorsnes, T., 2020. Revealing the secrets of Norway's seafloor – geological mapping within the MAREANO programme and in coastal areas. Geological Society, London, Special Publications.

Breiman, L., 2001. Random forests. Mach. Learn. 45, 5–32.

Breiman, L., Friedman, J.H., Olshen, R.A., Stone, C.J., 1984. Classification and Regression Trees. Belmont, Wadsworth.

Bremner, D., Demaine, E., Erickson, J., Iacono, J., Langerman, S., Morin, P., et al., 2005. Output-sensitive algorithms for computing nearest-neighbour decision boundaries. Discrete Comput. Geom. 33, 593–604.

Brown, C.J., Smith, S.J., Lawton, P., Anderson, J.T., 2011. Benthic habitat mapping: a review of progress towards improved understanding of the spatial ecology of the seafloor using acoustic techniques. Estuar. Coast. Shelf Sci. 92, 502–520.

Brown, C., Beaudoin, J., Brissette, M., Gazzola, V., 2019. Multispectral multibeam Echo sounder backscatter as a tool for improved seafloor characterization. Geosciences 9.

Burrough, P.A., McDonell, R.A., 1998. Principles of Geographical Information Systems. Oxford University Press, New York.

Calvert, J., Strong, J.A., Service M, McGonigle, C., Quinn, R., 2015. An evaluation of supervised and unsupervised classification techniques for marine benthic habitat mapping using multibeam echosounder data. ICES J. Mar. Sci. 72, 1498–1513.

Carlotto, M.J., 2009. Effect of errors in ground truth on classification accuracy. Int. J. Remote Sens. 30, 4831–4849.

Congalton, R.G., 1991. A review of assessing the accuracy of classifications of remotely sensed data. Remote Sens. Environ. 37, 35–46.

Conrad, O., Bechtel, B., Bock, M., Dietrich, H., Fischer, E., Gerlitz, L., 2015. System for automated geoscientific analyses (SAGA) v. 2.1.4. Geosci. Model Dev. 8, 1991–2007.

Cortes, C., Vapnik, V., 1995. Support-vector networks. Mach. Learn. 20, 273–297.

Davies, C., Moss, D., Hill, M., 2004. EUNIS Habitat Classification Revised 2004. European Environment Agency, European Topic Centre on Nature Protection and Biodiversity, Paris.

Diesing, M., Mitchell, P., Stephens, D., 2016. Image-based seabed classification: what can we learn from terrestrial remote sensing? ICES J. Mar. Sci. 73, 2425–2441.

Diesing, M., Mitchell, P.J., O'Keeffe, E., Gavazzi, G.O.A.M., Bas, T.L., 2020. Limitations of predicting substrate classes on a sedimentary complex but morphologically simple seabed. Remote Sens. 12, 3398.

EMODnet Digital Bathymetry (DTM 2020). EMODnet Bathymetry Consortium.

Enwright, N.M., Wang, L., Wang, H., Osland, M.J., Feher, L.C., Borchert, S.M., et al., 2019. Modeling Barrier Island habitats using landscape position information. Remote Sens. 11.

Foody, G.M., 2002. Status of land cover classification accuracy assessment. Remote Sens. Environ. 80, 185–201.

Freeman, T.G., 1991. Calculating catchment area with divergent flow based on a regular grid. Comput. Geosci. 17, 413–422.

Gaida, T.C., Mohammadloo, T.H., Snellen, M., Simons, D.G., 2019. Mapping the seabed and shallow subsurface with multi-frequency multibeam echosounders. Remote Sens. 12.

Gallant, J.C., Dowling, T.I., 2003. A multiresolution index of valley bottom flatness for mapping depositional areas. Water Resour. Res. 39.

Georgian, S.E., Anderson, O.F., Rowden, A.A., 2019. Ensemble habitat suitability modeling of vulnerable marine ecosystem indicator taxa to inform deep-sea fisheries management in the South Pacific Ocean. Fish. Res. 211, 256–274.

Goodman, A.J., Walker, T.R., Brown, C.J., Wilson, B.R., Gazzola, V., Sameoto, J.A., 2020. Benthic marine debris in the bay of fundy, eastern Canada: spatial distribution and categorization using seafloor video footage. Mar. Pollut. Bull. 150, 110722.

Guinan, J., McKeon, C., O'Keeffe, E., Monteys, X., Sacchetti, F., Coughlan, M., et al., 2021. INFOMAR data supports offshore energy development and marine spatial planning in the Irish offshore via the EMODnet geology portal. Q. J. Eng. Geol. Hydrogeol. 54.

Guisan, A., Weiss, S.B., Weiss, A.D., 1999. GLM versus CCA spatial modeling of plant species distribution. Plant Ecol. 143, 107–122.

Harris, P.T., Baker, E.K., 2012. Why map benthic habitats? In: Harris, P.T., Baker, E.K. (Eds.), Seafloor Geomorphology as Benthic Habitat. Elsevier, London, pp. 3–22

Hasan, R., Ierodiaconou, D., Monk, J., 2012. Evaluation of four supervised learning methods for benthic habitat mapping using backscatter from multi-beam sonar. Remote Sens. 4, 3427–3443.

Howe, J.A., Stevenson, A., Gatliff, R., 2015. Seabed mapping for the 21st century – the marine environmental mapping programme (MAREMAP): preface. Earth Environ. Sci. Trans. R. Soc. Edinb. 105, 239–240.

Ierodiaconou, D., Schimel, A.C.G., Kennedy, D., Monk, J., Gaylard, G., Young, M., et al., 2018. Combining pixel and object based image analysis of ultra-high resolution multibeam bathymetry and backscatter for habitat mapping in shallow marine waters. Mar. Geophys. Res. 39, 271–288.

Iwahashi, J., Pike, R.J., 2007. Automated classifications of topography from DEMs by an unsupervised nested-means algorithm and a three-part geometric signature. Geomorphology 86, 409–440.

Janowski, L., Trzcinska, K., Tegowski, J., Kruss, A., Rucinska-Zjadacz, M., Pocwiardowski, P., 2018. Nearshore benthic habitat mapping based on multi-frequency, multibeam echosounder data using a combined object-based approach: a case study from the rowy site in the southern Baltic Sea. Remote Sens. 10, 1983.

Janowski, L., Kubacka, M., Pydyn, A., Popek, M., Gajewski, L., 2021. From acoustics to underwater archaeology: deep investigation of a shallow Lake using high-resolution hydroacoustics—the case of Lake Lednica, Poland. Archaeometry. https://doi.org/10.1111/arcm.12663 (In press).

Jarna, A., Baeten, N.J., Elvenes, S., Bellec, V.K., Thorsnes, T., Diesing, M., 2019. Semi-automatic versus manual mapping of cold-water coral carbonate mounds located offshore Norway. ISPRS Int. J. Geo Inf. 8.

Jasiewicz, J., Stepinski, T.F., 2013. Geomorphons — a pattern recognition approach to classification and mapping of landforms. Geomorphology 182, 147–156.

Jenness, J.S., 2004. Calculating landscape surface area from digital elevation models. Wildl. Soc. Bull. 32, 829–839.
Kotilainen, A.T., Kaskela, A.M., Bäck, S., Leinikki, J., 2012. 17 - submarine de geer moraines in the Kvarken Archipelago, the Baltic Sea. In: Harris, P.T., Baker, E.K. (Eds.), Seafloor Geomorphology as Benthic Habitat. Elsevier, London, pp. 289–298.
Kursa, M., 2016. Robust and Efficient Approach to Feature Selection With Machine Learning. Faculty of Mathematics, Informatics and Mechanics. University of Warsaw.
Kursa, M.B., Rudnicki, W.R., 2016. Package 'Boruta'. Wrapper Algorithm for All Relevant Feature Selection.
Landis, J.R., Koch, G.G., 1977. The measurement of observer agreement for categorical data. Biometrics 33, 159–174.
Lecours, V., Dolan, M.F.J., Micallef, A., Lucieer, V.L., 2016. A review of marine geomorphometry, the quantitative study of the seafloor. Hydrol. Earth Syst. Sci. 20, 3207–3244.
Lu, D., Weng, Q., 2007. A survey of image classification methods and techniques for improving classification performance. Int. J. Remote Sens. 28, 823–870.
Lucieer, V., Pederson, H., 2008. Linking morphometric characterisation of rocky reef with fine scale lobster movement. ISPRS J. Photogramm. Remote Sens. 63, 496–509.
Lyons, M.B., Keith, D.A., Phinn, S.R., Mason, T.J., Elith, J., 2018. A comparison of resampling methods for remote sensing classification and accuracy assessment. Remote Sens. Environ. 208, 145–153.
MacMillan, R.A., Shary, P.A., 2009. Chapter 9 Landforms and Landform Elements in Geomorphometry. Geomorphometry - Concepts, Software, Applications, pp. 227–254.
Masetti, G., Mayer, L., Ward, L., 2018. A Bathymetry- and Reflectivity-Based Approach for Seafloor Segmentation. 8, p. 14.
Mayer, L., Jakobsson, M., Allen, G., Dorschel, B., Falconer, R., Ferrini, V., et al., 2018. The nippon Foundation—GEBCO seabed 2030 project: the quest to see the World's oceans completely mapped by 2030. Geosciences 8, 1–18.
Misiuk, B., Lecours, V., Dolan, M.F.J., Robert, K., 2021. Evaluating the suitability of multi-scale terrain attribute calculation approaches for seabed mapping applications. Mar. Geod. 1–30.
Mitchell, P.J., Downie, A.-L., Diesing, M., 2018. How good is my map? A tool for semi-automated thematic mapping and spatially explicit confidence assessment. Environ. Model Softw. 108, 111–122.
Montereale Gavazzi, G., Madricardo, F., Janowski, L., Kruss, A., Blondel, P., Sigovini, M., et al., 2016. Evaluation of seabed mapping methods for fine-scale classification of extremely shallow benthic habitats – application to the Venice lagoon, Italy. Estuar. Coast. Shelf Sci. 170, 45–60.
Montereale-Gavazzi, G., Roche, M., Lurton, X., Degrendele, K., Terseleer, N., Van Lancker, V., 2018. Seafloor change detection using multibeam echosounder backscatter: case study on the belgian part of the North Sea. Mar. Geophys. Res. 39, 229–247.
Pearman, T.R.R., Robert, K., Callaway, A., Hall, R., Iacono, C.L., Huvenne, V.A.I., 2020. Improving the predictive capability of benthic species distribution models by incorporating oceanographic data – towards holistic ecological modelling of a submarine canyon. Prog. Oceanogr. 184, 102338.
Porskamp, P., Rattray, A., Young, M., Ierodiaconou, D., 2018. Multiscale and hierarchical classification for benthic habitat mapping. Geosciences 8.
Proudfoot, B., Devillers, R., Brown, C.J., Edinger, E., Copeland, A., 2020. Seafloor mapping to support conservation planning in an ecologically unique fjord in Newfoundland and Labrador, Canada. J. Coast. Conserv. 24.
Pydyn, A., Popek, M., Kubacka, M., Janowski, L., 2021. Exploration and reconstruction of a medieval harbour using hydroacoustics, 3-D shallow seismic and underwater photogrammetry: a case study from Puck, southern Baltic Sea. Archaeol. Prospect. https://doi.org/10.1002/arp.1823 (In press).
Rende, S.F., Bosman, A., Di Mento, R., Bruno, F., Lagudi, A., Irving, A.D., et al., 2020. Ultra-high-resolution mapping of Posidonia oceanica (L.) delile meadows through acoustic, optical data and object-based image classification. J. Mar. Sci. Eng. 8.
Riley, S.J., De Gloria, S.D., Elliot, R., 1999. A terrain ruggedness that quantifies topographic heterogeneity. Intermountain J. Sci. 5, 23–27.
Rudowski, S., Wroblewski, R., Dworniczak, J., Szefler, K., Hac, B., Gajewski, L., 2019. Subaqueous geomorphology: options, tasks, needs. Bull. Geophys. 16, 89–97.
Ryabinin, V., Barbière, J., Haugan, P., Kullenberg, G., Smith, N., McLean, C., 2019. The UN decade of ocean science for sustainable development. Front. Mar. Sci. 6.
Sappington, J.M., Longshore, K.M., Thompson, D.B., 2007. Quantifying landscape ruggedness for animal habitat analysis: a case study using Bighorn sheep in the Mojave Desert. J. Wildl. Manag. 71, 1419–1426.
Schmidt, J., Hewitt, A., 2004. Fuzzy land element classification from DTMs based on geometry and terrain position. Geoderma 121, 243–256.
Shang, X., Robert, K., Misiuk, B., Zhao, J., Mackin-McLaughlin, J., 2021. Self-adaptive analysis scale determination for terrain features in seafloor substrate classification. Estuar. Coast. Shelf Sci. 254.
Sowers, D.C., Masetti, G., Mayer, L.A., Johnson, P., Gardner, J.V., Armstrong, A.A., 2020. Standardized geomorphic classification of seafloor within the United States Atlantic canyons and continental margin. Front. Mar. Sci. 7.
Story, M., Congalton, R.G., 1986. Accuracy assessment: a user's perspective. Photogramm. Eng. Remote. Sens. 52, 397–399.
Todd, B.J., 2016. De Geer moraines on German Bank, southern Scotian shelf of Atlantic Canada. J. Geol. Soc. Lond. Mem. 46, 259–260.
Trimble, 2014. Trimble Documentation: eCognition Developer 9.0 Reference Book. Trimble Germany GmbH, Munich, Germany.
Trzcinska, K., Janowski, L., Nowak, J., Rucinska-Zjadacz, M., Kruss, A., Schneider von Deimling, J., et al., 2020. Spectral features of dual-frequency multibeam echosounder data for benthic habitat mapping. Mar. Geol. 427, 106239.
Walbridge, S., Slocum, N., Pobuda, M., Wright, D., 2018. Unified geomorphological analysis workflows with benthic terrain modeler. Geosciences 8, 94.
Wölfl, A.-C., Snaith, H., Amirebrahimi, S., Devey, C.W., Dorschel, B., Ferrini, V., et al., 2019. Seafloor mapping – the challenge of a truly Global Ocean bathymetry. Front. Mar. Sci. 6.
Wood, J., 1996. The Geomorphological Characterisation of Digital Elevation Models. University of Leicester.
Zelada Leon, A., Huvenne, V.A.I., Benoist, N.M.A., Ferguson, M., Bett, B.J., Wynn, R.B., 2020. Assessing the repeatability of automated seafloor classification algorithms, with application in marine protected area monitoring. Remote Sens. 12.
Zevenbergen, L.W., Thorne, C.R., 1987. Quantitative analysis of land surface topography. Earth Surf. Process. Landf. 12, 47–56.
Zieger, S., Stieglitz, T., Kininmonth, S., 2009. Mapping reef features from multibeam sonar data using multiscale morphometric analysis. Mar. Geol. 264, 209–217.
Zwolak, K., Wigley, R., Bohan, A., Zarayskaya, Y., Bazhenova, E., Dorshow, W., et al., 2020. The autonomous underwater vehicle integrated with the unmanned surface vessel mapping the southern Ionian Sea. the winning technology solution of the Shell Ocean discovery XPRIZE. Remote Sens. 12, 1344.